MAGNETIC-ACTUATED ELECTROSPUN SHAPE MEMORY MATS

by

Xirui Wang

A THESIS SUBMITTED IN PARTIAL FULFILLMENT OF

THE REQUIREMENTS FOR THE DEGREE OF

MASTER OF APPLIED SCIENCE

in

THE FACULTY OF GRADUATE AND POSTDOCTORAL STUDIES

(Materials Engineering)

THE UNIVERSITY OF BRITISH COLUMBIA

(Vancouver)

October 2014

Abstract

Shape memory materials are the materials that can be deformed and fixed to a temporary shape and recover their original shape on exposure to external stimulus. Shape memory properties have been widely used for various applications such as actuators, adaptive mateirals and so on. This study firstly imparts this special property to nanofibers in light of various advantages including nanoporous structure, excellent recoverability and good biocompatibility. Then magnetite nanoparticles are incorporated into this system to realize the magnetic actuation of shape memory effect. In the first stage, poly (ε-caprolactone)-based polyurethane nanofibers were successfully fabricated by means of electrospinning. Through cyclic tensile testing, it was shown that in comparison with shape memory bulk films, the polyurethane shape memory nanofiber nonwovens had better shape recovery ability ascribed to molecular orientation. In the second stage, magnetite was successfully incorporated into polyurethane shape memory mats through the sonic mixing and subsequently the electrospinning process. SEM images showed that the fibers became more uniform and the diameter increased after magnetite incorporation. Differential scanning calorimetry and dynamic mechanical analysis revealed that the magnetite-incorporated mats still featured the melting transition which was similar with the pure mats, providing the magnetite-incorporated mats large possibilities to have shape memory effect. Through cyclic tensile testing, the recovery ratio decreased slightly because incorporated magnetite nanoparticles damaged the polyurethane matrix continuity. Moreover, electrospun mats with 5 wt%, 7.5 wt%, and 10 wt% magnetite were able to be heated to above their transition temperatures under a magnetic field with strength of 0.03T and frequency of 410 kHz. Helix recovery directly demonstrated that shape memory effect of magnetite-incorporated

electrospun mats could be triggered under a specific magnetic field. Magnetic-actuated electrospun shape memory mats hold great potential for biomedical applications such as scaffolds in tissue engineering and drug delivery matrix in drug releasing system.

Preface

All the experimental design and the data analysis were done by myself. All the experiments were conducted by myself in the Advanced Fibrous Materials Laboratory at University of British Columbia expect for these five experiments. The experiment in Section 3.3.2 was conducted in the Bioimaging lab at University of British Columbia. The experiment in Section 3.3.3 was done in the Hydrometallurgy lab at University of British Columbia. The experiment in Section 3.3.6 was conducted in the Fuel Cell Research Laboratory at Simon Fraser University. Section 3.3.8 and section 3.3.9 were based on information provided by Dr. Silvio Dutz who is the Head of the Magnetic Nanoparticles Group at the Institute of Biomedical Engineering and Informatics in Germany.

A version of Chapter 4 was published as a conference poster in the Society of the Advancement of Materials and Process Engineering (SAMPE) conference at Seattle in June 2-5, 2014. The co-authors Dr. Yuqin Wan and Dr. Frank Ko provided advices to me about the conducted experiments and data analysis in this poster.

Conference Poster:

Xirui Wang, Yuqin Wan and Frank Ko, "Polyurethane Nanofiber Nonwovens with Shape Memory Property", *the Society of the Advancement of Materials and Process Engineering (SAMPE) conference*, Seattle, Washington, the United States, June 2-5, 2014.

Table of Contents

List of Tables

List of Figures

List of Symbols

Symbol	Definition	Unit
T_g	the glass transition temperature	℃
T_m	the melting point	℃
ε_m	the stretched strain in the cyclic tensile testing	%
ε_u	the strain after unloading at room temperature	%
ε_p	the residual strain after recovery	%
R_r	the recovery ratio	%
R_f	the fixity ratio	%
ΔH	enthalpy data	J/g
M_R	remanent magnetization	T
H_c	coercivity	T

List of Abbreviations

BDO	1,4-butanediol
CNTs	carbon nanotubes
DMA	dynamic mechanical analysis
DMF	dimethylformamide
DSC	differential scanning calorimetry
Fe3O4	iron (II, III) oxide (magnetite)
MDI	methylene diphenyl diisocyanate
MWCNTs	mutil-walled carbon nanotubes
NiTi	nickel-titanium alloy
SMAs	shape memory alloys
SMPs	shape memory polymers
PBAG	poly (1,4-butylene adipate) glycol
PCL	poly (ε-caprolatone)
PCO	polycyclooctene
PEA	poly (ethylene adipate)
PEG	poly (ethylene glycol)
PEO	poly (ethyleneoxide)
PET	polyethylene terephthalate
PLA	poly (lactic acid)
PMMA	poly (methyl methacrylate)
PPDL	poly (ω-pentadecalactone)
PTFE	polytetrafluoroethylene

PUs	polyurethanes
PVAc	poly (vinyl acetate)
SEM	scanning electron microscopy
SMPUs	shape memory polyurethanes
SMFs	shape memory fiber
TEM	transmission electron microscopy
TGA	thermogravimetric analysis
XRD	x-ray diffraction measurement

Acknowledgements

I offer my enduring gratitude to Dr. Frank Ko at University of British Columbia who inspired and guided me in this field. I owe particular thanks to Dr. Yuqin Wan at University of British Columbia who answered my questions and provided me with consistent assistant. I would also thank Dr. Rizhi Wang and Dr. Goran Fernlund for reviewing my thesis and giving me valuable suggestions.

I would thank the Advanced Fibrous Materials lab and the Department of Materials Engineering which provided me equipment and space for conducting experiments and studying. I would like to thank Merquinsa Company and Dr. Angel Marcos at Spanish National Research Council in Spain for providing materials. I would offer many thanks to Dr. Silvio Dutz at the Institute of Biomedical Engineering and Informatics in Germany, Dr. Erik Kjeang and Dr. Marc-Antoni Goulet at Simon Fraser University, and Dr. Garnet Martens and Mr. Bradford Ross in Bioimaging Lab at University of British Columbia who provided me with equipment and helped me conduct experiments. I would also thank Dr. Jacob Kabel who gave me advices about imaging and data analysis.

I would like to acknowledge The Canada Foundation for Innovation (CFI) and The Natural Science and Engineering Research Council of Canada (NSERC) for financial support.

I would also like to extend my warmest thanks to my labmates and officemates who supported encouraged me whenever I encountered problems. Special thanks are owed to my parents, whose have supported me throughout my years of education, both morally and financially.

Dedication

To my parents

Chapter 1: Literature Review

1.1 Shape Memory Effect

Shape-memory effect is an effect to memorize a macroscopic (permanent) shape. The materials with this effect are called shape memory materials. Shape memory materials have the ability to be manipulated to a temporary shape under specific conditions of temperature and stress, and then relax to the original shape upon application of external stimulus such as temperature, electric field, magnetic field and so on. As shown in Figure 1-1, the whole process includes two steps. During programming process, the material is fixed to the temporary shape. The process to actuate it back to the permanent shape is known as the recovery process. The important quantities to be determined for describing the shape-memory properties of the material are the recovery ratio R_r and the fixity ratio R_f. The recovery ratio quantifies the ability of the material to memorize its permanent shape during the recovery process and is a measure of how far the original shape can be recovered. The fixity rate describes the ability to fix the mechanical deformation during the programming process. It describes how exactly the temporary shape can be fixed after specific conditions of temperature and stress [1].

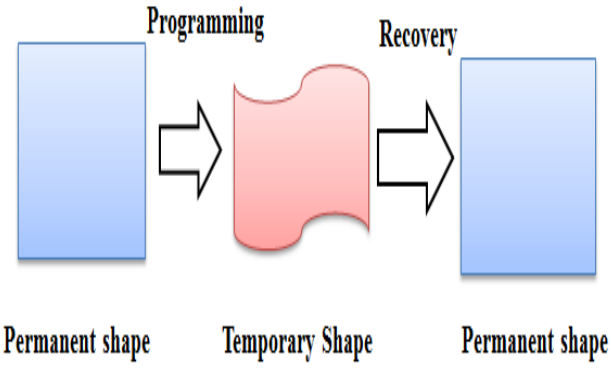

Figure 1-1: Schematic representation of shape memory effect

1.2 Shape Memory Alloys (SMAs)

The most widely used shape-memory materials in past years are shape-memory alloys (SMAs). SMAs were first observed in a AuCd alloy by Chang and Read in 1951.[2] However, the interest towards commercial applications was little until the shape-memory effect in the nickel-titanium alloy (NiTi, Nitinol alloys) was discovered by Buehler [3] in 1963. Currently, Nickel-titanium, copper-aluminum-nickel alloys and copper-zinc-aluminum-nickel are the three main kinds of SMAs.

The shape memory properties of SMAs are based on the crystal lattice change of a specific martensite variant to the parent single crystal phase. SMAs generally have two phases which are a high temperature-favored austenite phase and a low temperature-favored martensite phase. Therefore, metallic alloys change from austenite to martensite upon cooling and change from martensite to austenite when heating. During shape

recovery cycles, SMAs are firstly cooled down. Upon cooling, the phase transformation from austenite to martensite originally caused by shear lattice distortion leads to formation of several martensitic variants. Then the deformation stress is applied, giving rise to the transformation of the variants of other martensite phase into a specific variant of martensite phase. This results in the macroscopic shape change of the SMAs. Then heating actuates it switched to the austenite phase, ending up with the recovery of the original shape[1]. However, the recoverable deformation strain of SMAs is usually below 10%. Otherwise, the deformation will cause the slippage of the lattice, which is unrecoverable. The limited recoverable strain has become one of the biggest shortcomings of SMAs [2].

Shape Memory Alloys have been widely used for commercial applications. There are two aspects of SMAs leading to various applications. One aspect is the pseudo-elastic behavior when SMAs are used as frames including eye glass frames (bow bridges and temples) and frames for brassieres. Their shapes can be adjusted to fit the specific face or body, thus enhancing the wearing comfort.[4]

.

Another aspect of SMAs is recovery property which makes metallic alloys able to be actuated to the original shape under thermal, electrical or environmental command. Due to this special shape recovery effect, they are potential for a lot of applications such as actuators[5], adaptive materials in space area for vibration and shape control[6]and hybrid composites where SMAs are embedded to realize shape memory effect[4]. An example is an interesting design of smart dress using two-way SMA wires. The dress was

made of fabric embedded with SMA wires. When the dress was heated by using a hair dryer, it shrank up and shortened the dress. And the under sections recovered at a low temperature without hot air blowing.[7] This has potential to be used in intelligent clothing area.

1.3 Shape Memory Polymers (SMPs)

1.3.1 Advantages of Shape Memory Polymers

Despite the demonstrated merits, SMAs show some limitations for their application, such as the limited recoverable strains of less than 8%, high cost, a relatively inflexible transition temperature, and complex processing. Such limitations have provided motivations for the development of alternative materials, especially shape-memory polymers. The major advantages of shape memory polymers are given below:

1. Low density (e.g., the typical bulk density of a polyurethane SMP is 1.25 g/cm3 while that of a NiTi SMA is 6.4 g/cm3) and low cost raw materials.[8]

2. The relatively inexpensive fabrication of SMPs into complex shapes through various traditional and advanced polymer processing technologies such as extrusion, casting, injection molding or machining provides the possibility of specific device geometries required for different applications. [9]

3. They can reach large attainable strains. For certain polymers strains of up to 700% have been reported compared to less than 10%, 1%, and 0.1% for SMAs, SM ceramics, and glasses, respectively[10].

4. The actuation temperature can be tailored for specific applications by modifying the chemical compositions. For example, in the Poly (hexylene adipate)-based shape memory polyurethanes with various hard segment contents and soft segment lengths, their transition temperature changed from 41.0 to 51.9 ℃. [11]

5. SMPs can realize multi-shape recovery through multi-phase transitions. For example, in PMMA/PEG semi-interpenetrating polymer networks containing broadened glass transition and crystalline segments which provided multi-gradient glass transition temperatures and an additional melting temperature as transition temperatures, quintuple-step shape fixation and recovery were realized in a single shape memory cycle.[12] Multi-shape recovery can also be achieved by only one broad transition phase. The perfluorosulphonic acid ionomer which exhibited dual-, triple-, and at least quadruple-shape memory effects is one example. [13]

6. Their biocompatibility and even biodegradability open a door for SMPs to be applied in biomedical area such as minially invasive surgery. [9] [14][15]

1.3.2 Mechanism of Shape Memory Polymers

Since the shape memory effect of polymers is mostly triggered thermally, this study only focuses on thermally-induced shape memory polymers. Generally, SMPs are materials composed of two phases which are hard-segment-forming phase and soft-segment-forming phase. Figure 1-2 shows how the hard-segment-forming phase (shown in dark) and the soft-segment-forming phase (shown in red and blue) work in the thermally-induced SMPs. The hard-segment-forming phase can be the hard segments with physically cross-linkers (Figure 1-2 a) or chemical cross-linkers (Figure 1-2 b). The highest thermal transition is related to the hard-segment-forming phase. As long as this thermal transition is not exceeded, these domains will stabilize the permanent shape. The soft chain segments contain flexible components. The transition temperature is determined by the glass transition temperature or melting point of the soft segments. As shown in the first picture in Figure 1-2 a and b, above the transition temperature, soft segments would get into the rubbery or partly-melting state, leading to polymer networks exhibiting super-elasticity. At this point, the polymer chain segments are quite flexible, maintaining a maximum entropy before macroscopic deformation occurs. Upon application of deformation (such as extensition shown in Figure 1-2), the segments become oriented with a loss of entropy. When the polymers are cooled down below the transition temperature, the soft segments are partly limited because of the glassy or semi-crystalline state, ending up with the stability of the deformation (shown in the second picture in Figure 1-2 a and b). At the same time, the external stress has been stored. As soon as the temperature is back to above the transition temperature, the external stress

can be released and the segments can form random coils again because this conformation is entropy favored, resulting in recovery of the original shape (shown in the third picture in Figure 1-2 a and b).

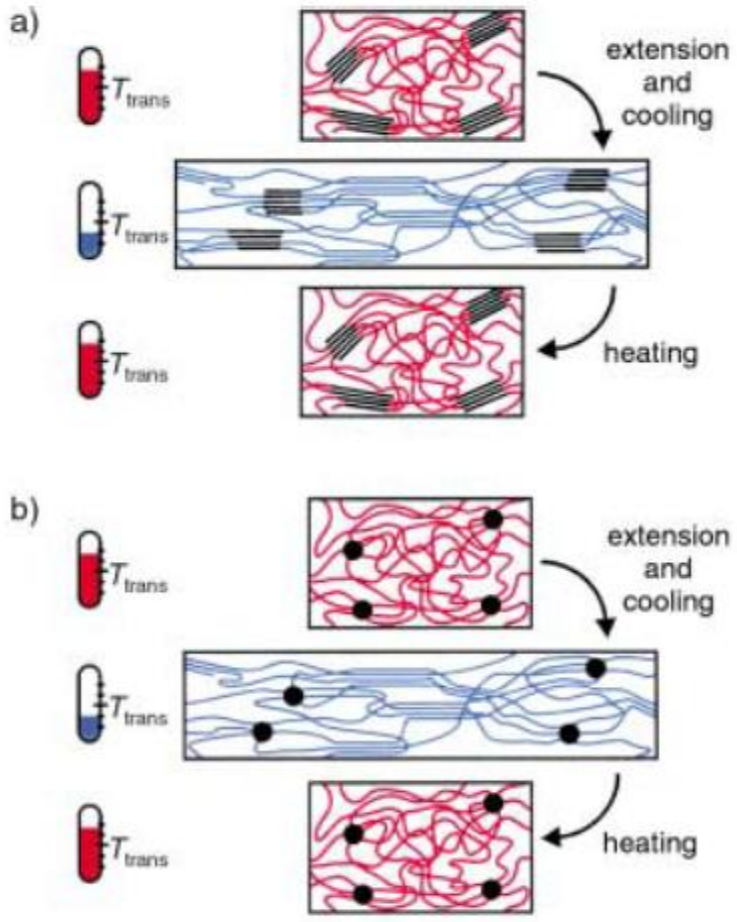

Figure 1-2: Schematic representation of the molecular mechanism of the thermally induced shape-memory effect for a) a physically cross-linked polymer with T_{trans} b) a covalently cross-linked polymer with T_{trans} (the flexible red part above T_{trans} and the fixed blue part below T_{trans} both represent the soft segment and the dark part stands for the hard segment)[1] (from © Andreas Lendlein & Steffen Kelch (2002). Shape-Memory Polymers. Angewandte Chemie International Edition, 41, 2034-2057. Page 2040. Adapted with permission from John Wiley and Sons)

1.3.3 Types of Shape Memory Polymers

In terms of the forming types of the hard-segment-forming phase, SMPs can be classified into chemically and physically cross-linked SMPs. The chemically cross-linked SMPs consider chemical cross-linkers as hard-segment-forming phase while the hard phase for physically cross-linked SMPs is hard segments with physical cross-linkers. In addition, for each type, they can be divided into two types according to the transition temperature which is either the glass transition temperature or the melting temperature of the soft segments.

1.3.3.1 Physically Cross-Linked Shape Memory Polymers

Generally, most of the physically cross-linked shape memory polymers are linear block copolymers which belong to thermoplastic polymers. This kind of material based on the formation of a phase-segregated morphology contains two segments that are hard and soft segments. The phase with the highest thermal transition is hard segment with physical cross-linking, providing the mechanical strength of the material as well as the stability of the permanent shape above the transition temperature. The phase with the lower thermal transition is the soft segment, determining the molecular transition during the shape memory process.

Compared with the thermo-set shape memory polymers, this class can be easily designed to different shapes and forms for various specific applications. Moreover, the existence of physical interactions decreases chain slippage during deformation and therefore increases the extent of shape recovery.

The most common physically cross-linked shape memory polymer is thermoplastic polyurethane (PU). Polyurethanes feature many unique properties including a wide range of shape recovery temperatures (from −30 to 70 °C), high shape recoverability, good processing ability and excellent biocompatibility[16][17][18]. Basically, polyurethanes are usually synthesized according to the pre-polymer method as shown in Figure 1-3. In this process, those difunctional, hydroxyl-terminated oligoesters or -ethers react with an excess of a low molecular weight diisocyanate to obtain isocyanate-terminated pre-polymers (Figure 1-3, 1st reaction step). Low molecular weight diols or diamines are then added as chain extenders to further couple these pre-polymer, ending up with thermoplastic polyurethanes or polyurethane-urea copolymers (Figure 1-3, 2nd reaction step).

Because of the immiscibility between the hard segment and the soft segment, polyurethanes undergo micro-phase separation. [19] The segment that contains urethane and urea bonds linked through chain-extender molecules is considered as hard segments. The strong intermolecular interactions of hydrogen bondings between the hard-hard segments [20] act as physical cross-linkers, leading to the capability of hard segments to stabilize the permanent shape above the transition temperature. In the meantime, the

hard-segment forming phase is embedded in an amorphous elastic matrix which is composed of polyesters or polyethers. This amorphous phase is the soft segment which provides transition temperature , resulting in the shape memory effect.

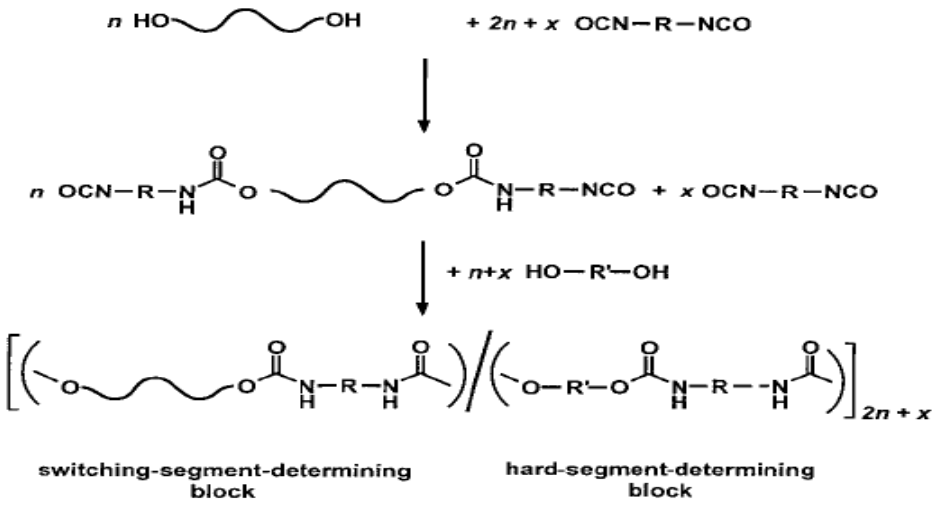

Figure 1-3: Schematic representation of pre-polymerization process of polyurethane [1](from © Andreas Lendlein & Steffen Kelch (2002). Shape-Memory Polymers. Angewandte Chemie International Edition, 41, 2034-2057. Page 2043. Adapted with permission from John Wiley and Sons)

1.3.3.1.1 Linear Block Copolymers with $T_{tran}=T_g$

Linear block copolymer is the phase separated materials whose transition temperature is the glass temperature. T_g-based polyurethane is one of the examples. The polyurethanes synthesized from diphenylmethane diisocyanate (MDI), poly (ethy1ene adipate) (PEA) as soft segments, 1,4-butanediol (BDO) as chain extender were reported to have shape memory effect. [16] The transition temperature ranged from 10-50 ℃ which was affected by the molecular weight of the soft segment and MDI/PEA/BDO mole ratio.

Besides hydrogen bonding in polyurethane system, other physical cross-linked techniques can also be used to set the network such as crystalline domains. For example, in a blend of poly(vinyl acetate) (PVAc) and poly(lactic acid) (PLA)[21], those crystalline domains served as hard segments and the composition-dependent T_g of the amorphous region functioned as the transition temperature. This kind of material could be processed and reshaped when the temperature was above the melting point of these crystalline domains.

1.3.3.1.2 Linear Block Copolymers with $T_{tran}=T_m$

For some block copolymers, the soft domain will crystallize and the temporary shape is fixed by crystallization of the soft domains. Therefore, in this case, the transition temperature is attributed by the melting point of semi-cystalline soft segments.

The common example is Tm-based segmented polyurethane. Semi-crystalline poly-caprolactone diols (PCL) [22] or Poly(1,4-butylene adipate) glycol (PBAG) [23] are often chosen as soft segments. A lot of research has been focused on the improvement of recovery property. For example, ionic group [24], cationic group [25] or long alkyl chains [23] were incorporated into the polyurethane system to enhance micro-phase separation. Another example is the introduction of a rosin-based chain extender into the hard segment of the SMPUs to improve the phase separation and stability of the hard segment domains at the same time [26].

Besides T_m-based polyurethanes, there are still other linear, phase-separated block copolymers with the transition temperature ascribed to melting of soft segments. A thermoplastic copolymer with a hard-segment-forming phase based on PET and switching-segment blocks of PEO[27] is an example. Depending on the molecular mass of the PEO blocks, the transition temperature can be varied between 40 ℃ and 60 ℃.

1.3.3.2 Chemically Cross-Linked Shape Memory Polymers

Basically, chemically cross-linked polymers are also thermoset polymers. They can be divided into T_g-based thermoset shape memory polymers and T_m-based ones as follows in terms of different types of soft segments. The strong chemical cross-linking provides this kind of polymer especially the T_g-based one some attractive characteristics that include excellent degree of shape recovery, intrinsically high modulus and great thermal and chemical stability.[10] However, once the original shape is fixed, it is unable to be changed because the chemical cross-linking is not reversible, which limits the applications of thermoset polymers. In addition, chemically cross-linked polymers cannot be dissolved in solvent very well.

1.3.3.2.1 Thermoset Networks with $T_{tran}=T_g$

The simplest type of shape-memory polymer is a chemically cross-linked glassy polymer. The chemical cross-links support the original shape of the system as net-points while the

soft chains changes between the glassy and rubbery state below and above the glass transition temperature.

An example of this class is polystyrene copolymers which were a reaction product of styrene, a vinyl compound, a multifunctional cross-linking agent and an initiator [28]. They were used as contact lens molds. Besides, polymers having T_g that was above room temperature accompanied with ultra-high molecular weight which was at least higher than 10^6 g/mol may also be included in this category because they featured a significant number of entanglements per chain which functioned as cross-links [2]. Among this kind of polymers, the most widely known one is high molecular weight poly(methyl methacrylate) [29]. The glass transition temperature was around 105 ℃. Such polymers showed almost complete shape fixing and recovery which resulted from the sharp glass-transition temperature and high entanglement density that formed a three dimensional network.

1.3.3.2.2 Thermoset Networks with $T_{tran}=T_m$

The melting transition of semi-crystalline polymers can also be employed to trigger shape recovery. And the temporary shape is fixed by crystallization instead of vitrification. Compared with glassy materials, this kind is generally more compliant below the transition temperature since the stiffness is sensitive to the degree of crystallinity. This class of materials includes semi-crystalline polymers, liquid-crystal elastomers, and hydrogels with crystalline microdomains [2].

For example, chemically cross-linked polycyclooctene (PCO) was developed as a novel polymeric shape memory system [30]. The original stress-free shape was recovered within 1s on immersion in hot water above the melting point of the crystalline phase, which demonstrated its fast shape recovery behavior. And the transition temperature could be tailorable by means of changing the trans/cis ratio of vinylene groups. Besides, recently, Jianlian Hu and co-workers[31] introduced one kind of shape memory polyurethane, which was cross-linked by excess MDI or by glycerin, and found that this chemically cross-linked SMPUs had better thermal and thermo-mechanical properties than those prepared from linear polyurethanes due to strong chemical bonding.

However, as for T_m-based thermo-set SMPs, chemical cross-linking in a semi-crystalline material impedes crystal formation, probably ending up with a reduction of crystallinity and broader crystal-size distribution. So it might feature a lower melting point and a broader transition temperature range.

1.3.4 Applications of Shape Memory Polymers

Because of various advantages of shape memory polymers, they have become more and more popular and applied in different areas. Traditional applications include energy storage [32], the active disassembly of modern mobile phones [33], deployable hinge [34] and so on.

What's more, the recent applications are mainly focused on medical areas due to their good biocompatibility along with their wide range of tunable stiffness, tailorable transition temperatures, large shape deformation and easy processing. For example, it can be applied as a self-expandable stent [35]. The stent is tubular which is inserted into a natural passage/conduit in the body to prevent or counteract a disease-induced, localized flow constriction. The stent was firstly fixed to a constricted one which had a smaller diameter than the conduit below the transition temperature. It was then inserted into the passage. When the temperature of this stent reached the body temperature which was above the actuation temperature, it could recoil to fit the passage. The transition temperature could be low enough so it would recoil faster at the body temperature.

Degradable shape-memory suture was tested in a rat.[36]. The wound was loosely sutured with a standard surgical needle. When the temperature increased to 41℃, the shape-memory effect was actuated and the fiber shrank, which assured the closure of the wound.

Controlled drug release has also been on the list of the functionalities of shape memory polymers. They hold great potential as drug delivery matrix during the drug releasing process. Before inserted into body, this device was fixed into the temporary shape and then cooled down. After heated to above the switching transition temperature, it recovered to the primary shape when drug release happened. In addition, Wischke [37] also found out that there was no influence of incorporating drugs on the polymers glass

transition or the elastic properties in aqueous environment, which increased the possibility for the future applications as self-anchoring implants with a local drug release.

1.4 Shape Memory Fibers (SMFs)

1.4.1 Advantages of Shape Memory Fibers

In order to apply shape memory polymers into different specific areas, they are supposed to be processed into various forms such as membranes for self-deployable structures[8] [38], foams for memory pillows, memory mattresses, insoles [39] or embolic treatment of aneurysms [40] and gels for surface patterning techniques through swelling and shrinking [41].

In the past ten years, more and more research has been focused on a new form of shape memory polymers which are shape memory fibers in light of their several advantages including better mechanical property and recoverability due to molecular orientation [42], soft structure, excellent permeability [43] and good biocompatibility.

Dr. Hu successfully fabricated shape memory fibers in micro scale through wet spinning and melt spinning [44][45]. Moreover, using the fibers through wet spinning, shape memory fabrics were developed by knitting and weaving[46][47]. It was shown that the shape memory fabric was not cytotoxic, hemolytic, sensitive, or irritant, which means that it was more compatible with human bodies. [43] This kind of shape memory fabric

extended the applications of shape memory properties into the textile area. For example, the garments made of SMP fibers can be enlarged suitably to fit the wearer's body configuration because of the deformability and fixity of SMP fibers into temporary shapes [39]. Additionally, a melt-spun shape memory poly(ethylene terephthalate)–poly(ε-caprolactone) block copolymer was reported to be made into the automotive seatbelt fabric which can effectively improve a passenger's safety by absorbing the kinetic energy due to damping effect [39].

In recent years, many research groups chose to study shape memory nanofibers or ultrathin microfibers instead of regular shape memory microfibers. The preference of shape memory nanofibers is based on special properties of nanofibers.

1) Their great surface area to volume ratio can bring better mechanical properties, faster actuation [48] and a good handle [39].

2) Shape memory nanofibers are more biomimetic and biocompatible because a material with nanoroughness more accurately resembles native tissue [49]. This may make them more suitable for biomedical applications such as drug delivery systems[50], wound dressing [51] and so on. Besides, the antibacterial property can be realized in the polyurethane core-shell nanofibers through coaxial electrospun of the core solution of polycaprolactone-based shape memory polyurethane and shell solution of pyridine containing polyurethane. This special

property is due to the amido-group-containing shell materials and the high surface area of nanofibers. [52]

3) Furthermore, based on their unique structures, shape memory nanofibers can be applied in some specific applications which other forms are unable to realize. For example, nanofibrous structures meet the essential design criteria of an ideal tissue engineered scaffold due to its capability of supporting cell attachment and proliferation [53][54]. Moreover, these special structures, accompanied with shape memory properties, can realize the cell morphology control. When the scaffold is stretched and fixed to the temporary elongated shape, the fibers are aligned by the strain. After actuation, it is back to the initial shape and random fiber orientation. Since the behavior of attached and viable cells is directed by the fiber alignment, stem cell morphology can be controlled through fixing and recovery of shape memory scaffold. [55] Another special aspect of the structures is their numerous nanosized pores which provide excellent water vapor permeability [56] Due to the tunable pores of shape memory polyurethane nanofiber membranes [57] and an increase of water vapor permeability as the temperature rises [58], shape memory nanofibers hold great potential for intelligent protective clothing materials[59] [60].

1.4.2 Types of Polymers Used for Shape Memory Fibers

Shape memory fibers can be produced using the physically cross-linked shape memory polymers because physically cross-linked SMPs can be easily dissolved in solvent in comparison with thermo-set SMPs. Among the thermoplastic shape memory polymers, the most common ones are shape memory polyurethanes due to various advantages including a wide range of shape recovery temperatures, high shape recoverability and good processing ability[16][17][18]. In terms of monomers, 4,4'-diphenylmethane diisocyanate (MDI) is often chosen as diisocyanate in this system because it's the least toxic chemical among diisocyanates. 1,4-butanediol is utilized as the chain extender. However, as for the polyester diol or polyether diol, there are different choices. Therefore, based on soft segments, shape memory polyurethanes spun to be shape memory fibers can be divided to T_m-based shape memory polyurethanes and T_g-based shape memory polyurethanes.

In terms of T_m-based polyurethanes fibers, many research groups [44][57][60][61][62][63] utilized poly(ε-caprolactone) as soft segments to obtain T_m-based polyurethane fibers through various spinning techniques including electrospinning, melting spinning and wet spinning. Their preference is based on the advantages of T_m-based shape memory polymers and the strengths of poly(ε-caprolactone) as soft segments, which contains two aspects: 1) In terms of T_m-based shape memory polymers, they show a narrow transition zone while T_g-based ones feature a broad transition temperature range [64]. 2) As for poly(ε-caprolactone), it is a biodegradable polyester with a relatively low

T_m around 60 °C, and medical devices containing poly(ε-caprolactone) have been safely used in humans [65]. The PCL-based shape memory polyurethanes fabricated by different groups all showed good shape memory property. Their fixity ratio and recovery ratio were all above 80% and many of them were even above 90% [48][61][62][44][63]. In order to improve the shape recovery ratio and recovery force, Qinghao [66] prepared Mutil-walled carbon nanotubes (MWCNTs)-incorporated shape memory polyurethane fibers through in situ polymerization and melt spinning. The preferentially aligned MWCNTs in the fiber axial direction could help storing and releasing the internal elastic energy during stretching and relaxation. The incorporation of MWCNTs was also realized through coaxial electrospinning of the polyurethane core solution and the polyurethane-MWCNTs sheath solution to enhance mechanical property and shape recovery sensitivity [67]. Besides PCL-based shape memory polyurethanes fibers, poly (ethylene glycol) (PEG) was co-polymerized as soft segments to obtain T_m-based polyurethane with good shape memory effect [45].

T_g-based shape memory polyurethanes fibers were also fabricated by some research groups because they are able to store more elastic energy and therefore have relatively better shape recovery properties. [64] It was reported that they could be prepared through wet spinning using poly (buthylene adipate) diols or poly (ethylene adipate) glycol as soft segments[42][68][69]. As well, through electrospinning, T_g-based polyurethane nanowebs with polyether-type soft segments composed of polypropylene glycol and polyethylene glycol showed a great shape memory effect (shape recovery ratio of at least 99% and shape fixity ratio of at least 94%) with controllable pore structures [70].

Obviously, polyurethanes are not the only polymers that can be made into shape memory fibers. For example, Fenghua[71] fabricated shape memory nanofibers through dissolving poly(ethyleneoxide) (PEO) in 5.0 wt% Nafion solution by electrospinning technique. Degradable multiblock copolymer consisting of crystallizable poly(ω-pentadecalactone) hard segments (PPDL) and PCL switching segments was electrospun into shape memory nonwoven fabric which exhibited good shape memory properties with strain recovery rates of 89–95% and strain fixity rates of 82–83% after the 2nd cycle. [72]

1.4.3 Fabrication of Shape Memory Fibers

In order to impart the shape memory effect of polymers to fibers, spinning processes are employed to get shape memory fibers. Electrospinning is often used to produce shape memory ultrafine fibers in nanoscale while the wet spinning and the melt spinning are utilized to obtain regular shape memory fibers in micro scale. Which kind of fiber is needed depends on the requirement of fiber scale for specific applications.

1.4.3.1 Electrospinning

Electrospinning is a process that produces continuous nanofibers or ultrathin microfibers through an external electric field imposed on a polymer solution [59].

Most of the experimental work is carried out with the apparatus shown in Figure 1-4. Before spinning starts, the syringe containing polymer solutions connected to a stainless steel capillary tube (spinneret) is fixed. A high-voltage supply is connected to the capillary tube. The polymer fluid suspended from the capillary tube is held by its surface tension. Then high voltage is switched on. An electric field subjected to the spinneret induces a charge on the surface of the liquid. Mutual charge repulsion gives rise to a repulsive electrostatic force opposite to the surface tension. With increasing the intensity of electric field, the hemispherical surface of the fluid at the tip of the tube forms a conical shape known as the Taylor cone. And the intensity of this electric field is still increased until a critical value is reached when the repulsive electrostatic force overcomes the surface tension and a charged jet of fluid is ejected from the tip of the Taylor cone. The polymer solution jet then undergoes a whipping process when the solvent is evaporated, turning itself into fiber. Then the fibers reach the ground collector covered by the aluminum foil and lay themselves randomly on the foil. [54][73]

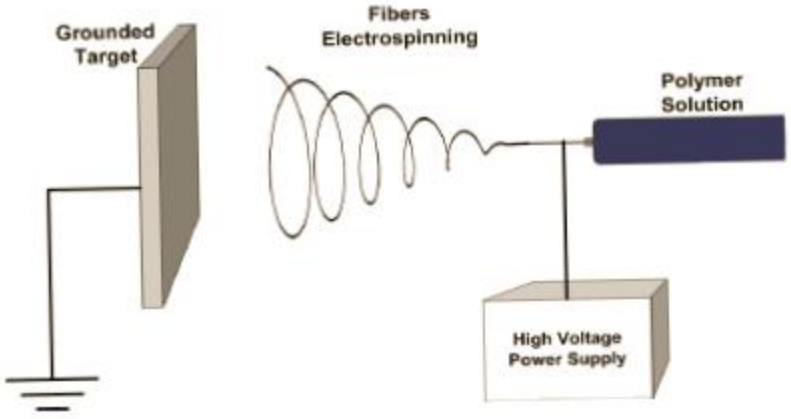

Figure 1-4: Schematic diagram of the electrospinning unit

1.4.3.2 Wet Spinning

Wet spinning is the oldest and the most complex process to produce fibers [59]. As shown in figure 1-5, this process is used for polymers that need to be dissolved in a solvent to be spun. The dope solution is poured into the stainless steel dope tank. A pump is then used to force the solution into a spinneret. The solution is extruded through spinneret capillary holes submerged horizontally in a coagulating bath where the solvent is diffused out. Multi-filaments are then formed by coagulation. After passing through the coagulation bath, the filaments are taken and then passed through a water bath to remove the residual DMF. They are then dried in hot air and winded into the original fibers. [68][69] [74]

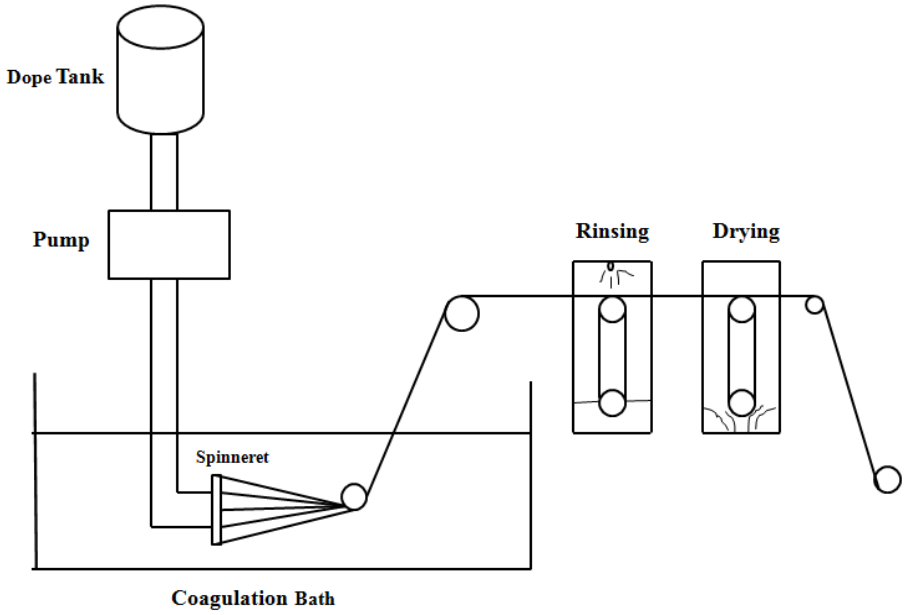

Figure 1-5: Schematic diagram of the wet spinning equipment

1.4.3.3 Melt Spinning

Melt spinning is used for thermoplastic polymers that can be melted without heavy degradation. As shown in Figure 1-6, the polymer pellets are melted in an extruder. The melten polymers then flow into a spin pack by pump. After being extruded from the spinneret, the polymers solidify by cooling and form into multi-filaments. Then, the filaments are further solidified and winded to the fibers [75][76].

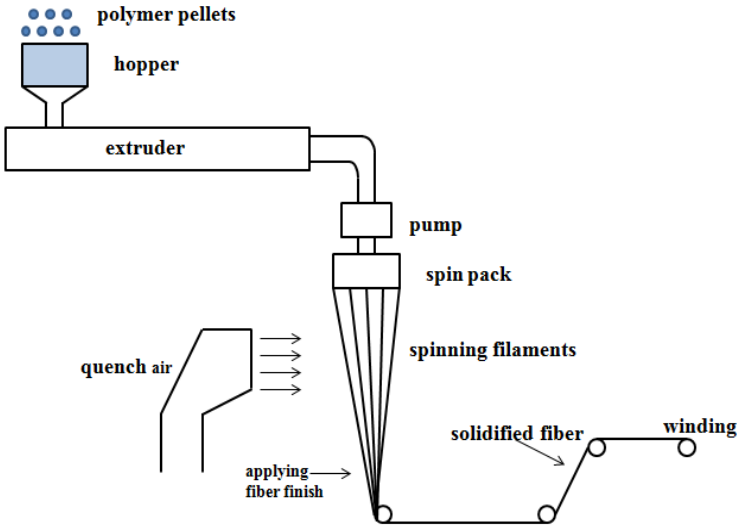

Figure 1-6: Schematic diagram of the melt spinning equipment

Melt spinning has several advantages such as no harmful solvent, no need for coagulation bath, and is economical [76]. And Qinghao Meng and co-workers [62] found melt-spun SMFs had higher tenacity, breaking elongation and shape memory effect compared with those of wet-spun SMFs. Because it had higher phase separation, resulting in both better

soft segment and hard segment crystallization. However, the shape memory polyurethanes for the melt spinning should have high thermal stability and relatively high molecular weight to obtain good mechanical properties.

1.5 Various Actuation Methods of Shape Memory Effect

The majority of SMPs are thermally-induced shape memory polymers whose shape memory effect is actuated by heat. Besides direct heating, several heating schemes use external energy sources to selectively heat the SMPs. Therefore, there are various actuation methods to stimulate shape memory effect.

1.5.1 Direct Heating

Direct heating is a good method to trigger the shape memory effect of devices mostly in our daily life such as the active disassembly of mobile phones and so on. In the biomedical area, when the transition temperature is close to the body temperature, body heat can be considered as a direct heating method to accomplish the actuation [9]. In some cases, even if the transition temperature is above the body temperature, the body heat can also be used for triggering the shape recovery as long as the complete recovery is not required. For example, a shape memory electrode with the transition temperature of 70 ℃ was actuated by body heat and self-inserted into the nervous system after initial surgical implantation of the device. While the complete recovery was not obtained, the heat from the body lead to appropriate slow actuation of the probe back to its original conformation, which was better for insertion [77].

However, as for the biomedical devices, the transition temperature being a little bit higher than the body temperature may be desired because they would bring more mechanical rigidity at body temperature as well as explicit control of the actuation [9]. Therefore, body heat is not enough for complete recovery. But direct heating on the body would damage tissues. This provides motivations for finding other methods to generate heat. Moreover, there are some other special situations where direct heating is inconvenient such as space engineering. Therefore, alternative actuation methods to produce heat are necessary.

1.5.2 Electrical Actuation

These electrical sensitive SMPs can be obtained by incorporating electrical conductive ingredients, such as conductive wires and carbontubes, into thermal active SMPs [78]. When a current passes through the conductive ingredient network within SMPs, the induced Joule heating may raise the internal temperature to above the transition temperature to trigger shape recovery. Dr. Cagri Ayranci realized electrical actuation of thermoset epoxy system by incorporating reinforcing carbon fibers[79]. The reinforcing carbon fibers increased shape recovery forces largely at the same time [80]. Qinghao Meng and his coworkers [81] incorporated multi-walled carbon nanotubes into shape memory fibers, obtaining electro-active shape memory fibers with 75% shape recovery ratio. Sravendra Rana[82] fabricated core-sheath polyurethane nanofibers coated with conducting polymers polypyrrole and poly (3-hexylthiophene). It was demonstrated that the conducting core-sheath structured webs were effective in generating sufficient electrical heating necessary for featuring the shape memory effect.

However, the necessity of a direct contact to the material by electrodes and the lack of biocompatibility strongly restrict the use of these systems in biological environments. [83]

1.5.3 Photothermal Actuation

Light can also trigger shape recovery by generating heat. For example, Ward Small [84]obtained shape memory polymers doped with indocyanine green dye used as a laser-activated microactuator for thrombus removal. This SMP microactuator in its temporary straight rod form was first inserted through a catheter distal to the vascular occlusion. By absorption of laser light, the temperature increased and this microactuator then transformed into its original corkscrew shape, enhancing capturing the thrombus. Once deployed, the microactuator was retracted, along with the captured thrombus being removed from the body. The blood flow was then restored. [85] Besides laser heating, the internal temperature can also be raised on exposure to infrared sources. After incorporating carbon nanotubes, the shape memory effect of the thermoplastic elastomer Morthane was triggered by the absorption of non-radiative decay of infrared photons of carbon nanotubes. At the same time, a higher recovery stress was yielded by incorporation of carbon nanotubes. [86]

1.5.4 Magnetic Actuation

The heat can also be generated in a magnetic way due to the hysteresis loss. When ferromagnetic nanoparticles are exposed to an external magnetic field, they become magnetized. However, the relationship between field strength H and magnetization M is

not linear in such materials. As shown in Figure 1-7, starting from the point when this material is demagnetized (H=M=0), as the field strength increases, M follows the initial magnetization curve. This curve increases rapidly at first and then approaches an asymptote called magnetic saturation. If the magnetic field is now reduced monotonically, M follows a different curve. At zero field strength, the material is still magnetized with an amount called remanent magnetization M_R. And the field strength to decrease magnetization to zero is called coercivity H_c. Therefore, when the field strength bounced within a range, their magnetization undergoes a closed loop: the hysteresis loop. The area within the loop measures the magnetic energy delivered in the form of heat to the material with the magnetic particles. The energy conversion to heat is caused by the coupling of the atomic magnetic moments to the crystal lattice.[87] [88] [89]

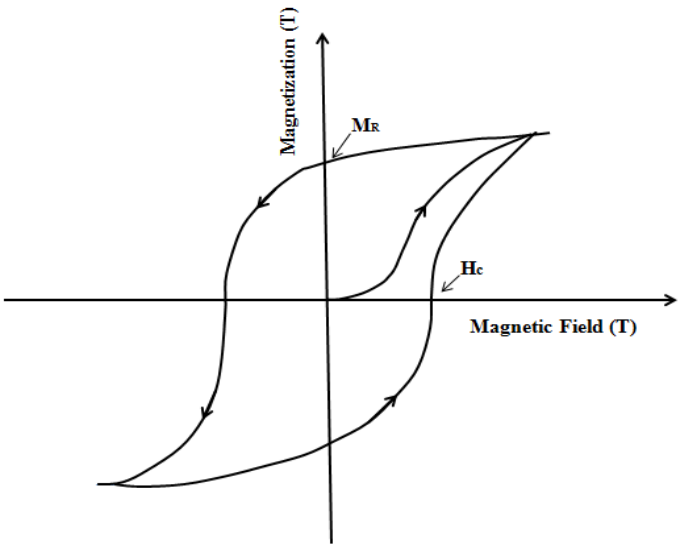

Figure 1-7: The curve of the magnetic hysteresis loop

Currently, research has demonstrated magnetic actuation of shape memory effect in thermoset polymers [90][91] as well as thermoplastic polymers [92]. In terms of ferromagnetic nanoparticles, magnetite nanoparticles are the most common ones because they are non-toxic and biodegradable. [83][93] In order to strengthen materials at the same time, Tao Gong and his coworkers applied multi-walled carbon nanotubes (MWNTs) coated with Fe_3O_4 nanoparticles as the incorporated fillers [94]. Yan Cai crosslinked polyurethane composites filled with Fe_3O_4 nanoparticles with multi-walled carbon nanotubes (MWCNTs) [95]. To move this area forward, triple shape was achieved by non-contact actuation in an alternative magnetic field [96]

In comparison with the electrical and photothermal actuation, magnetic actuation is preferred especially for biomedical applications because of the following reasons.

1) Remote actuation which allows for the possibility of actuating implantable devices later by an external magnetic field, opening the door for an entirely new class of SMP devices later under a magnetic field such as drug delivery matrix in drug releasing system and scaffolds in tissue engineering.
2) Eliminating fiber optics or wires and the connection of these items to a device simplify design and reduce the possibility of failure.
3) More complex device shapes can be achieved because consistent heating is expected for any type of device geometry. As for traditional laser and electro-resistive heating methods, device geometry is limitd by the requirement of correct light refraction/absorption and thermal conduction. [97]
4) Magnetic nanoparticles can be non-toxic and biodegradable [94].

Chapter 2: Objective

Even though there is some research about shape memory fibers as well as multiple actuation methods of shape memory effect, there are few work focused on indirect heating of shape memory nanofibers. Therefore, based on previous work, the major objective of this study is to realize magnetic actuation of shape memory nanofibers. In order to reach this goal, the work is divided into two stages which are: a) preparation and characterization of the general shape memory nanofiber nonwovens and b) fabrication and characterization of magnetite-incorporated electrospun shape memory nonwovens.

a) To fabricate and characterize the general shape memory nanofiber nonwovens

Before magnetic actuation, pure shape memory nanofibers need to be studied. In this part, nanofiber nonwovens are to be fabricated followed by the study of morphology, thermal properties, thermo-mechanical properties and shape memory properties of shape memory nonwovens. Furthermore, all the properties of nanofibers would be compared with those of regular shape memory films to demonstrate the strengths of nanofibers.

b) To study the feasibility of magnetic actuation of shape memory nonwovens

This second is to reach the main goal of the work. Firstly, magnetite is to be incorporated into nanofiber nonwovens. Then the work would be focused on the effect of magnetite of different concentrations on morphology, thermal properties, thermo-mechanical properties and shape memory properties of nanofibers. More importantly, the feasibility of magnetic actuation of magnetite-incorporated shape memory nonwovens is to be explored.

Chapter 3: Materials and Methods

This chapter describes preparation of shape memory polymer films and fabrication of shape memory nanofiber nonwovens and magnetite-incorporated shape memory nanofiber nonwovens. Characterization techniques are also included in this chapter.

3.1 Materials

The shape memory polymers used in this work were poly(ε-caprolatone)-based polyurethanes (Merquinsa Pearlstick ® 45-40/19, 4.431×10^4 g/mol). The general structure of segmented polyurethanes is shown in Figure 1-3 and the chemical structure of poly(ε-caprolactone) diol which composed the soft segments is shown below in Figure Dimethylformamide (DMF) were purchased from Fisher Scientific. Magnetite nanoparticles with average diameter of 30 nm were purchased from Nanostructured & Amorphous Materials Inc. The surfactant Triton® X-100 were purchased from Sigma-Aldrich.

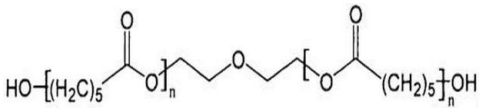

Figure 3-1: The chemical structure of poly(ε-caprolactone) diol

3.2 Preparation Process

3.2.1 Preparation of Shape Memory Polymer Films

The PU/DMF solution with concentration of 10 wt% was obtained after dissolving PU in DMF at room temperature. After spraying PTFE lubricante on the glass petri dish, the

solution was then poured into the petri dish. The bulk film was obtained after DMF had completely evaporated from the solution on the hot plate at 80 ℃ in the fume hood.

3.2.2 Fabrication of Shape Memory Nanofiber Mats

3.2.2.1 Solution Preparation

PU was dissolved in DMF at room temperature into 18 wt% solutions.

3.2.2.2 Electrospinning

Nanofiber nonwovens were fabricated using nanofiber electrospinning unit (Kato Tech Co. Ltd, Japan) The 10 ml syringe was set connected to a syringe pump. The voltage supplier was connected to the tip. The target for collecting fibers was covered by non-stick aluminum foil. The feed rate was controlled by the syringe pump and ranged from 0.05-0.1 mm/min. The voltage was from 12-16 kV. This was carried out at room temperature.

3.2.3 Fabrication of Magnetite-Incorporated Shape Memory Mats

3.2.3.1 Solution Preparation

PU was dissolved in DMF at room temperature into the PU/DMF solution with concentration of 22 wt%. Magnetite, the surfactant Ttrion X-100 and DMF were mixed together and sonicated in sonicator for half an hour. PU/DMF solution was then added into the final solution with concentration of 18 wt%. The whole solution was then sonicated for one more hour. Several solutions with different magnetite percentage of 2.5 wt%, 5wt%, 7.5wt%, and 10 wt% were obtained.

3.2.3.2 Co-Electrospinning

The electospinning process was similar with the one for fabrication of pure shape memory nanofiber nonwovens. The feed rate was controlled from 0.06-0.08 mm/min and the voltage was 11-15 kV. In the following chapter, nanofiber mats with magnetite concentrations of 2.5 wt%, 5 wt%, 7.5 wt%, and 10 wt% were called in the following chapters as mag-2.5, mag-5, mag-7.5, and mag 10, respectively.

3.3 Characterization Technique

3.3.1 Scanning Electron Microscope (SEM)

A scanning electron microscope (Hitachi S-3000N, Japan) was used to investigate the morphology of nanofibers and measure the diameter of nanofibers. The voltage was 10 kV and the working distance was around 15 mm. Images with different magnifications of 1K, 5K and 10K were obtained.

3.3.2 Transmission Electron Microscope (TEM)

The magnetite nanoparticles incorporated in the shape memory nowovens were observed through TEM (FEI, the Czech Republic). Single nanofibers were obtained on the foldable grid (the sample holder for TEM) during the electrospinning process when the grid was placed close to the collector. Then the holder was set inside the TEM equipment and images were obtained.

3.3.3 Thermogravimetric Analysis (TGA)

The magnetite nanoparticle content was determined using Perkin Elmer STA 6000 simultaneous thermal analyzer (USA) by complete combustion in nitrogen atmosphere from room temperature up to 600 ℃ in 10 ℃/min.

3.3.4 X-Ray Diffraction Measurement (XRD)

The investigation of the crystalline status of the samples was done by using an x-ray diffractometer (Rigaku Multiflex 2kW, Japan). It was conducted at a voltage of 40kV and a current of 20mA with copper k-alpha radiation. Spectra were obtained from 3 ° to 90 ° with a scanning rate of 1 °per minute.

3.3.5 Differential Scanning Calorimetry (DSC)

The thermal property of nanofibers was determined using DSC (TA Instruments Q1000, USA) During this process, the sample was heated up from -80 ℃ to 60 ℃ in 5 ℃/min and then cooled down to -80 ℃ in 2 ℃/min. And then it was heated up to 200 ℃. The second heating curve was taken as DSC heating curve shown in the results part.

3.3.6 Dynamic Mechanical Analysis (DMA)

The thermo-mechanical properties were investigated through DMA equipment (TA Instruments Q800, USA) operated in the tensile mode. The heating rate was 1 ℃/min, the frequency was 2 Hz, and the oscillation amplitude was 5.0 μm. The samples (20×8 mm) were tested over the temperature range from 10 to 70 ℃. The gauge length between the clamps was 10 mm.

3.3.7 Cyclic Tensile Testing

The shape-memory effect was quantified by cyclic investigations, which were performed by means of a tensile tester (Kato Tech Co. Ltd, Japan) equipped with a thermo-chamber, which is shown in Figure 3-1. Figure 3-2 shows the entire process of cyclic tensile testing and Figure 3-3 is the 3D represention of cyclic tensile testing (one cycle). The number showing the steps in both figures correspond to each other. Firstly, the test piece was heated up to 50 ℃ and was stretched to the strain ε_m (50% in my experiment). The sample was then cooled down under this constant strain ε_m to room temperature for 5 min. Then it was unloaded and the temporary strain ε_u was fixed. The sample was then heated up to 50 ℃ again in a controlled way. During this heating, it tried to recover to the original shape and ended up with the strain ε_p. And then next cyclic began. There were three cycles in total in my experiments.

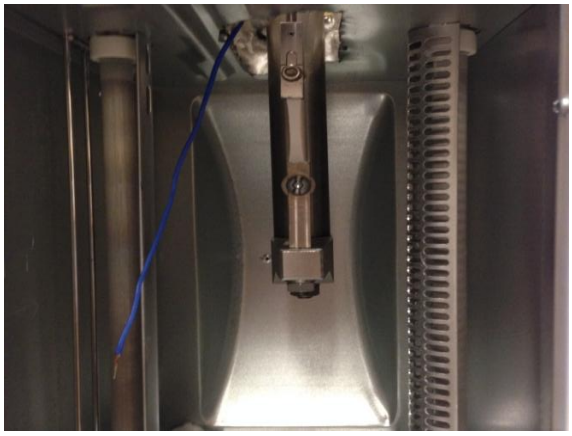

Figure 3-2: Experimental setup of tensile testing of samples around 50 ℃

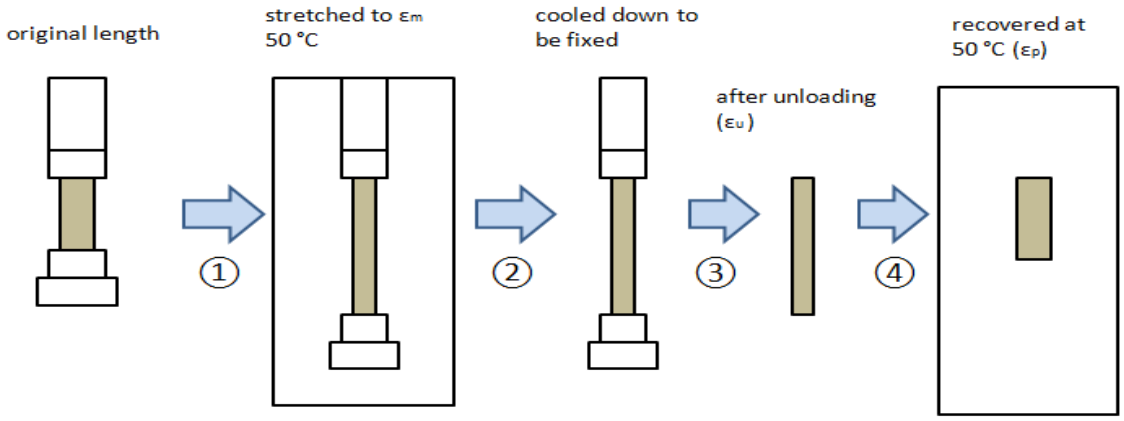

Figure 3-3: Schematic representation of cyclic tensile testing

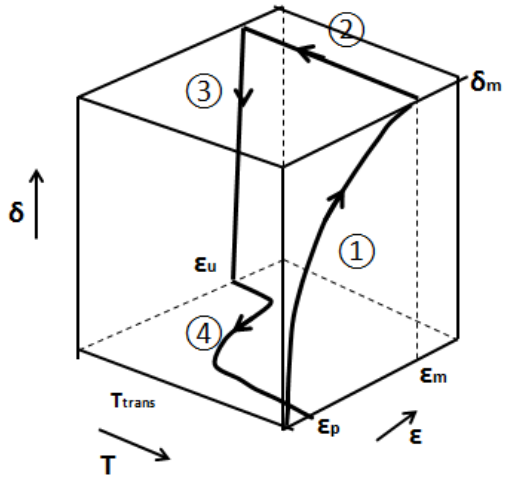

Figure 3-4: 3D representation of cyclic tensile testing

The important quantities which are strain recovery rate R_r and the strain fixity rate R_f can be calculated according to equations (1), (2), and (3) [1]from cyclic tensile testing.

The strain recovery rate R_r quantifies the ability of the material to memorize its primary shape. Therefore, it is the ratio of the recovered strain that occurs with the shape memory effect in the Nth cycle ε_m-$\varepsilon_p(N)$ to the stretched strain that occurs upon programming ε_m-$\varepsilon_p(N-1)$.

$$R_r(N) = [\varepsilon_m-\varepsilon_p(N)]/[\ \varepsilon_m-\varepsilon_p(N-1)] \quad (1)$$

$\varepsilon_p(N)$ and $\varepsilon_p(N-1)$ represent the strain of the sample in two successively passed cycles after shape recovery. The total strain recovery rate R_r is defined as the strain recovery after N passed cycles based on the original shape of the sample.

$$R_{r,tot}(N) = [\varepsilon_m-\varepsilon_p(N)]/\varepsilon_m \quad (2)$$

The strain fixity rate R_f describes the ability of the soft segment to fix the mechanical deformation during the programming process. Therefore, the strain fixity rate R_f is given by the ratio of the strain in the stress-free state after cooling and unloading in the Nth cycle $\varepsilon_u(N)$ and the programmed strain ε_m.

$$R_f(N) = \varepsilon_u(N)/\varepsilon_m \quad (3)$$

3.3.8 Magnetic Heating Testing

Magnetic heating was employed to observe the temperature increasing in nanofiber mats with magnetite of different concentrations under magnetic field with high frequency and strength within two minutes. The machine used was SINAC from EFD Induction in Germany. Firstly, the sample (10×10 mm) was placed within the coil. Then the field (H = 0.03T f = 410 kHz) was switched on. And the temperature was measured by means of a fiberoptic measurement system (FOTEMP, Germany) connected to the sample.

3.3.9 Helix Recovery under Magnetic Field

The visual demonstration of shape memory effect under magnetic field was done through helix recovery process. The nanofiber mat with 5 wt% magnetite (30×10 mm) was heated up to 50 ℃. Then this rectangular mat was deformed to be helix. It was then cooled down to room temperature and the helix was fixed for 10 min. And the helix was put within the coil and connected to the fiberoptic measurement system (FOTEMP, Germany). The field (H = 0.03T f = 410 kHz) generated by SINAC from EFD Induction in Germany was then switched on to heat the sample up. In order to avoid the temperature being up to so high, the maximal temperature was limited to 52 ℃. The whole recovery process was recorded.

Chapter 4: Characterization of Shape Memory Nanofiber Mats

This chapter is dedicated to polyurethane shape memory nanofiber mats. The morphology, thermo-mechanical properties and shape memory properties of nanofiber mats are discussed. Additionally, comparisons between nanofiber mats and films with various properties are also discussed.

4.1 Morphology of Shape Memory Nanofibers

Figure 4-1 b shows the SEM images of polyurethane nanofiber nonwovens fabricated using 18 % PU/DMF solution through electrospinning with 14.8 kV applied voltage and 0.076 mm/min. It was observed that no beads or agglomerations appeared on the nanofibers. It was also found that concentration was the main factor that influenced spinnability and morphology of nanofibers. The suitable range for the polyurethane in my work was 14-22%. There were beads on nanofibers (shown in Figure 4-1 a) when the concentration was too low while the high concentration led to high viscosity, which resulted in bigger diameters and increasing handling difficulties. As shown in Figure 4-1 d, the nanofibers were not so uniform and most of the diameters were 500-1000 nm with the average diameter being 720 nm.

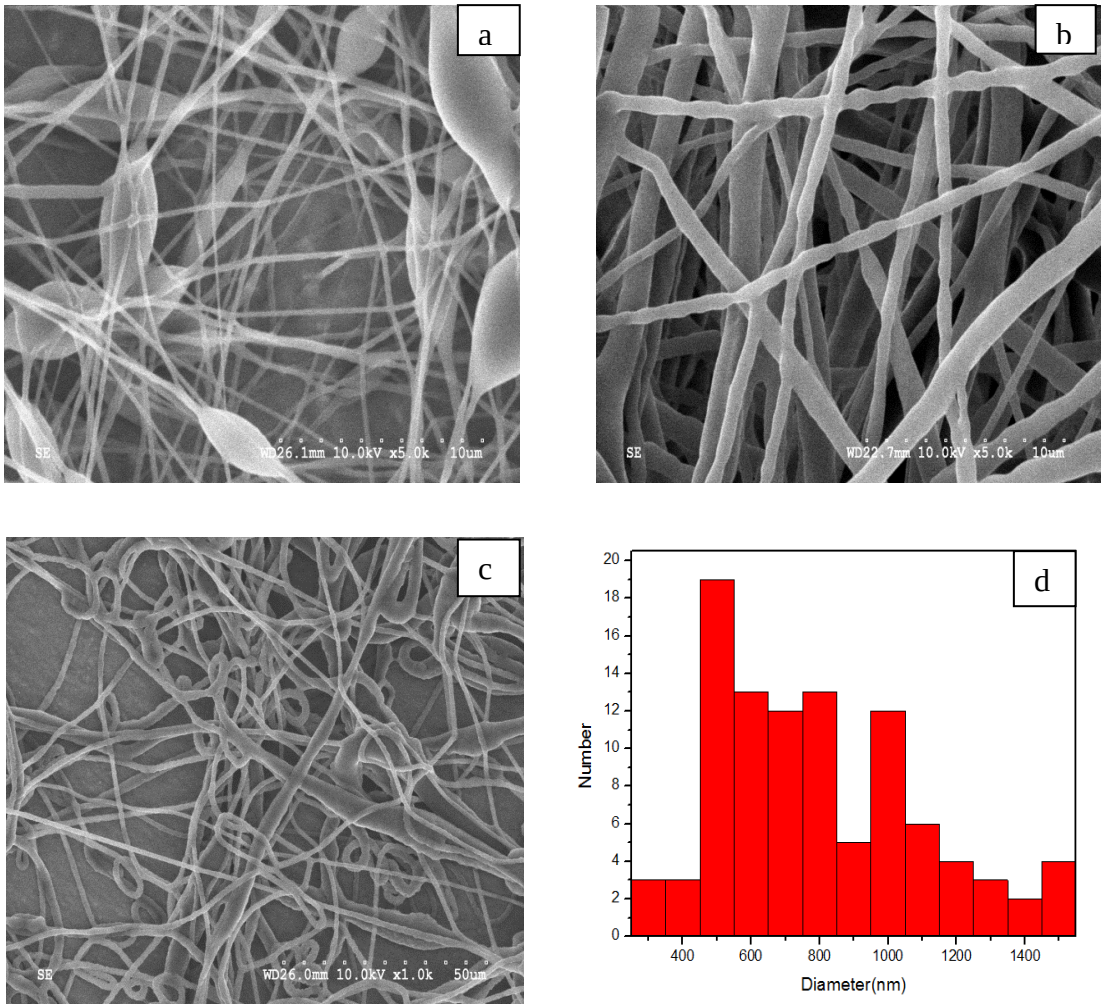

Figure 4-1: SEM images of Nanofiber Nonwovens from PU/DMF solutions with concentrations of a) 10% b) 18% c) 24%. d) the diameter distribution of nanofibers from 18% PU/DMF solution

4.2 Thermo-Mechanical Properties

4.2.1 Differential Scanning Calorimetry (DSC)

The endothermic melting peaks of soft segments respectively in nanofiber mats and films in the reheating (second heating) scan are shown in Figure 4-2. The peak of the nanofiber mat ascribed to the melting transition of soft segments was at 42.85 ℃ which was

slightly higher than that of film (41.96 ℃). The melting enthalpy of the nanofiber mat was 30.31 J/g while the enthalpy data of film was 28.67 J/g as shown in table 4-1. According to the reference[62], the higher soft-segment melting transition temperature suggests that the soft segments of nanofiber mats were of higher crystallinity. The larger melting enthalpy of the soft-segment phase suggests that more ordered polymer packaging was obtained in nanofiber mats. Since the crystallinity of the soft segment is responsible for the fixity of deformation [98], the fixity ratio of nanofiber mat might be higher. But because the difference was small, the obvious difference of fixity ratio between them was not expected.

An increase of heat capacity at around -40 ℃ is seen in both DSC curves. This was attributed to the glass transition of the soft segments [63][99]. Therefore, the semi-crystalline structure of soft segments was demonstrated by the DSC curves, satisfying the structural requirements of fibers having shape memory effect, as mentioned in chapter 1.

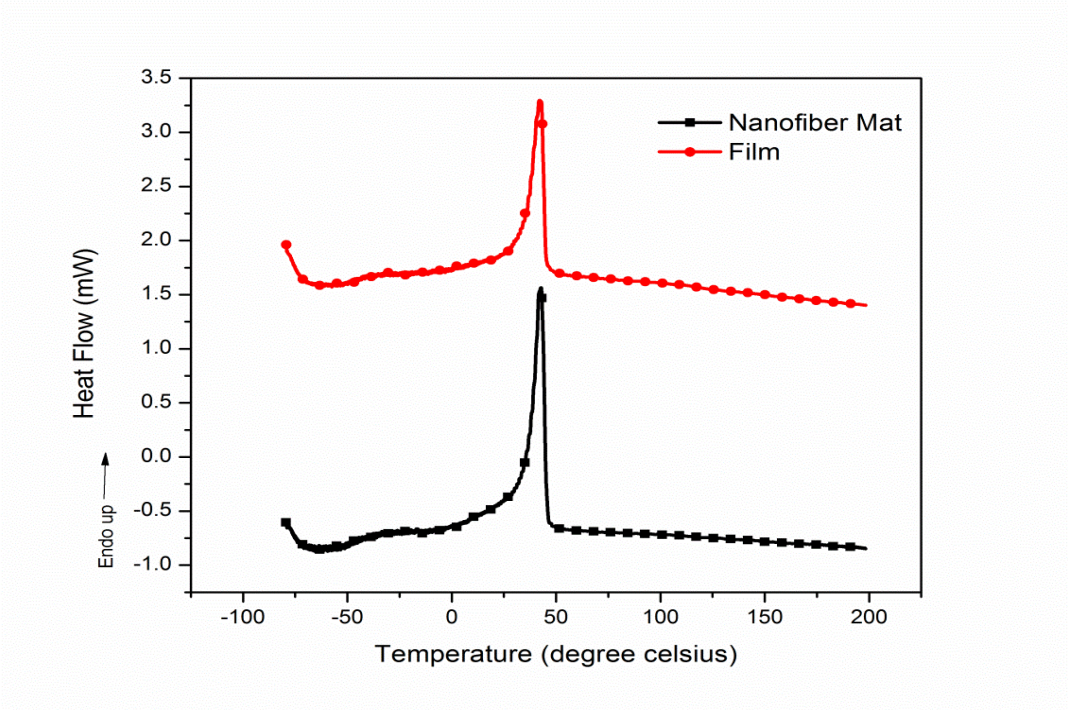

Figure 4-2: DSC curves of shape memory nanofiber mats and films

Table 4-1: DSC results of shape memory nanofiber mats and films

	T_m (℃ shown in DSC curve)	ΔH (J/g)
Nanofiber Mats	42.8	30.31
Films	41.9	28.67

4.2.2 Dynamic Mechanical Analysis (DMA)

Figure 4-3 presents the storage modulus of nanofiber mats and films during heating. It can be seen that the storage modulus had a large decreasing feature in both curves due to the melting transition of soft segments. Before the transition, the modulus was mostly attributed to physical cross-linking in hard segments and the crystalline portion of soft segments [100]. The modulus of films at this moment was approximately double that of the nanofiber mats because the strain during DMA tests was quite small and the nanofiber mats had a very low initial modulus compared to films due to the porous structure [60]. After the transition, the storage modulus became very low since the modulus was almost completely attributed by hard segments and the amorphous phase of soft segments. Therefore, besides DSC, DMA is also a method to demonstrate the melting transition of soft segments. The melting point measured from DMA curves is shown in table 4-2. As we can see, the melting point from DMA curves was similar with the DSC results. The dramatic decrease of the storage modulus caused by the melting transition of soft segments also provided the possibility for both nanofiber mats and films to have a shape memory effect.

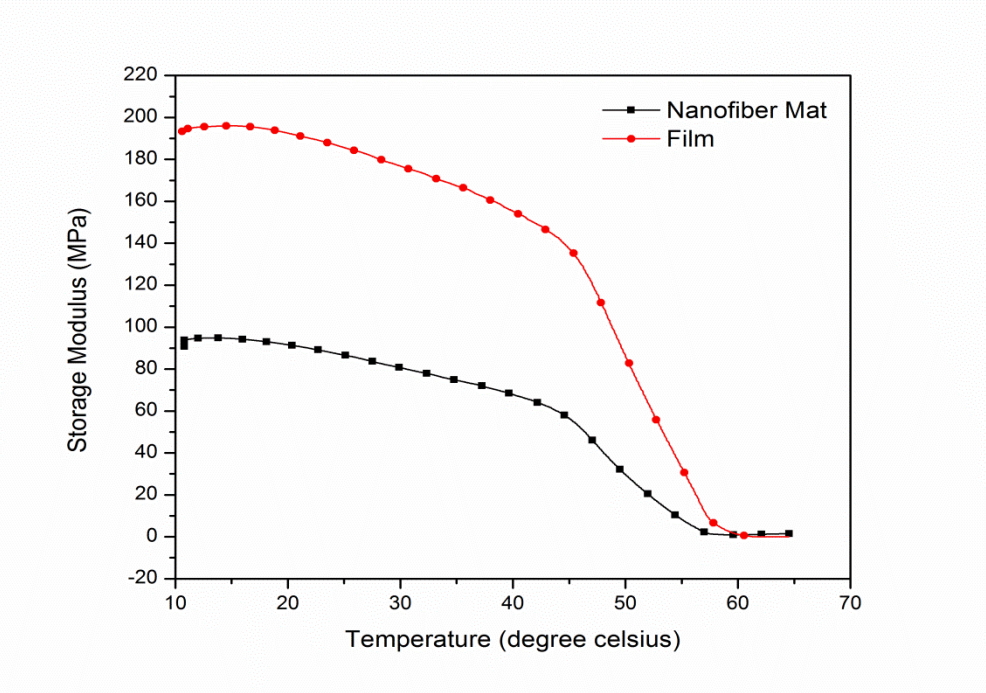

Figure 4-3: DMA curves of shape memory nanofiber mats and films

Table 4-2: DMA results of shape memory nanofiber mats and films

	T_m (℃ measured from DMA curves)	Storage Modulus at the beginning (MPa)	Storage Modulus after transition (MPa)
Nanofiber Mats	45.4	94.8	1.34
Films	44.3	196.7	1.13

4.3 Demonstration of Shape Memory Effect

In order to quantify the shape memory property, cyclic tensile tests were conducted. From the stress-strain curves shown in Figure 4-4, the shape recovery ratio and shape fixity ratio were calculated. As shown in table 4-3, the recovery ratio of nanofiber mats was higher than the one of films. This was because the molecular orientation resulted from the electrospinning process led to an increase in the amount of hard-segment phase along with stability enhancement of the physically cross-linked networks [42]. The shape recovery is mainly related to the stability of hard segment domains [60]. Thus, molecular orientation led to an increase of the shape recovery ratio. In terms of shape fixity ratio, films had slightly higher fixity ratio than electrospun mats. It might be because of the porous structure of electrospun mats.

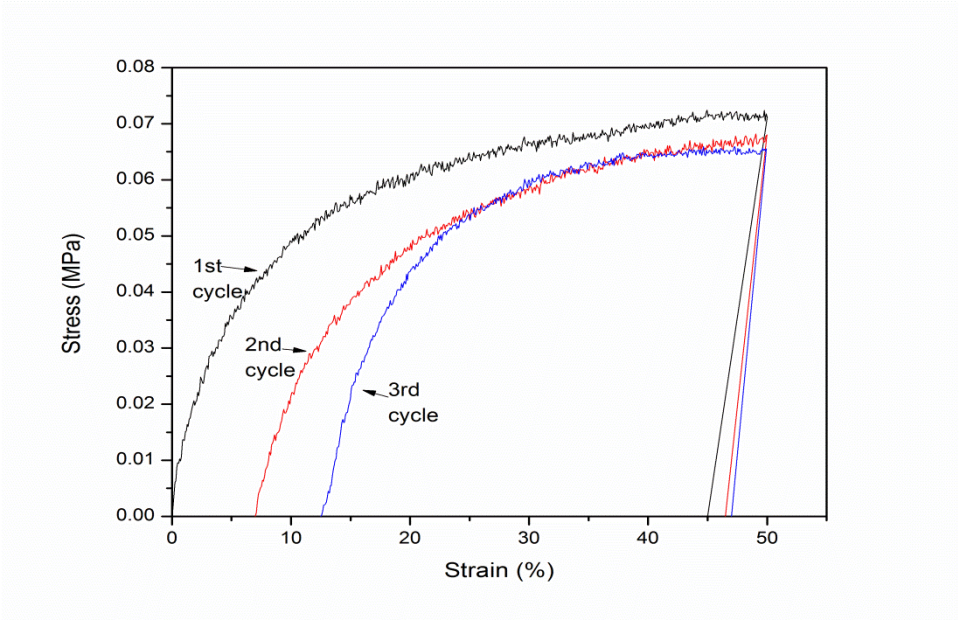

Figure 4-4: Cyclic tensile stress-strain curves of shape memory nanofiber mats

Here is the illustration of the shape memory effect accompanied with a phase change effect during cyclic tensile testing. When the sample was heated from room temperature to 50 ℃ (which was above the soft phase melting transition temperature T_{trans}) the PCL phase melted and became a random state. However, the fiber did not break as hard segments which were physically cross-linked, partly restricted the free movement of the soft segment phase. Upon application of external tension, the sample was stretched and the modulus was attributed to the physical cross-links and the amorphous part of soft segments. When the temperature was cooled to below T_{trans}, soft segments crystallized, which led to limited movements of the amorphous component in soft segments. As a result, internal stress was stored in the material and the associated deformation was fixed temporarily. When reheated to above T_{trans}, the PCL phase melted again and the amorphous phase turned back to random coils due to the entropy flavored. Therefore, the fiber returned to its original length with release of stored-up internal stress.

Table 4-3: Recovery ratio and fixity ratio of shape memory nanofiber mats and films

	Nanofiber Mats			Films		
	1st	2nd	3rd	1st	2nd	3rd
Recovery Ratio (%)	86 ±2	87 ±5	91 ±4	78 ±3	78 ±7	82 ±3
Fixity Ratio (%)	90 ±5	88 ±4	88 ±2	91 ±3	94 ±4	92 ±1

4.4 Conclusions

In this chapter, the polyurethane shape memory nanofiber mats produced through electrospinning were characterized. The average diameter was determined to be around 720 nm by means of scanning electron microscopy. Differential scanning calorimetry provided us with a slightly higher melting point and a larger melting enthalpy of nanofiber mat compared with film, and demonstrated the crystalline and amorphous phase in the soft phase. Through dynamic mechanical analysis, the storage modulus dramatically decreased, due to the melting point of the soft segments. Cyclic tensile testing revealed that nanofiber mats had better shape recovery ability ascribed to molecular orientation but with a slightly lower fixity ratio.

Chapter 5: Characterization and Magnetic Actuation of Magnetite-Incorporated Shape Memory Nanofiber Mats

This Chapter is focused on magnetite-incorporated shape memory nanofiber mats. The effects of magnetite on morphology, thermo-mechanical properties and shape memory properties of nanofibers are discussed. Furthermore, magnetic actuation of the shape memory effect is demonstrated.

5.1 Verification of the Existence of Magnetite

5.1.1 X-Ray Diffraction Measurement (XRD)

In order to prove the existence of magnetite, XRD was employed in this work, ending up with XRD curves shown in Figure 5-1. It can be observed that in all the curves there were two prominent peaks at angles of 21.36 ° and 23.65 °, and a broad peak around 20 °. According to the reference [101], the two prominent peaks were from crystallization of PCL (which was the soft segment in the mats) and the broad peak suggested the presence of an amorphous structure in soft phase. However, compared to the curve of pure mats, there were more peaks at 35.8 ° and 43.5 ° shown in magnetite-incorporated nanofiber mats. According to the magnetite XRD data file obtained from the XRD software, those peaks were attributed to the crystallization of magnetite nanoparticles, which demonstrated that magnetite was successfully incorporated into nanfiber mats.

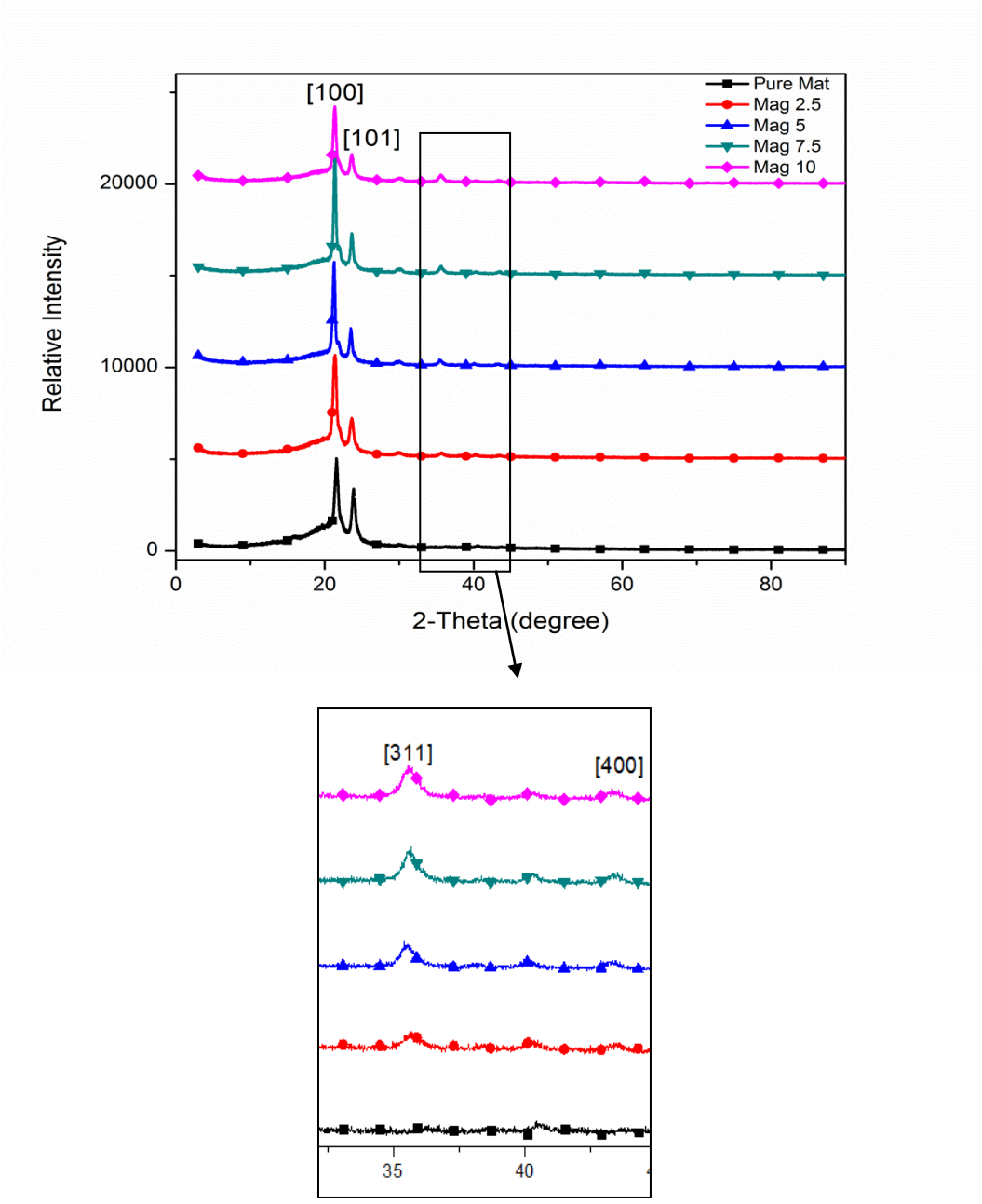

Figure 5-1: XRD curves of electrospun mats with magnetite of different concentrations

5.1.2 Thermogravimetric Analysis (TGA)

In order to know the concentration of magnetite in nanofiber mats, the samples were tested through TGA. The results are shown in table 5-1. The exact concentrations were all lower than the concentrations of magnetite incorporated into the mats because there was unavoidably a weight loss due to a small amount of magnetite remaining in the syringe during the electrospinning process. With concentration increasing, the difference between the concentration incorporated and the exact concentration in mats was bigger.

Table 5-1: Concentrations of magnetite in different nanofiber mats

	Mag 2.5	Mag 5	Mag 7.5	Mag 10
Concentration	2.46	4.41	6.37	8.38

5.2 Morphology of Magnetite-Incorporated Shape Memory Nanofibers

5.2.1 Scanning Electron Microscopy (SEM)

Figure 5-2 shows the SEM images of shape memory nanofibers with different concentrations of magnetite. It can be observed that magnetite-incorporated fibers were more uniform compared to the pure nanofibers. This might be because the electromagnetic induction generated by magnetite nanopaticles under electrical field enhanced the fiber orientation. Additionally, magnetite incorporation might limit the curving and winding of nanofibers, resulting in higher uniformity. Table 5-2 concluded the calculated average diameters of each nanofiber. The incorporation of magnetite

increased the diameter of nanofibers largely due to the higher viscosity and magnetite themselves inside.

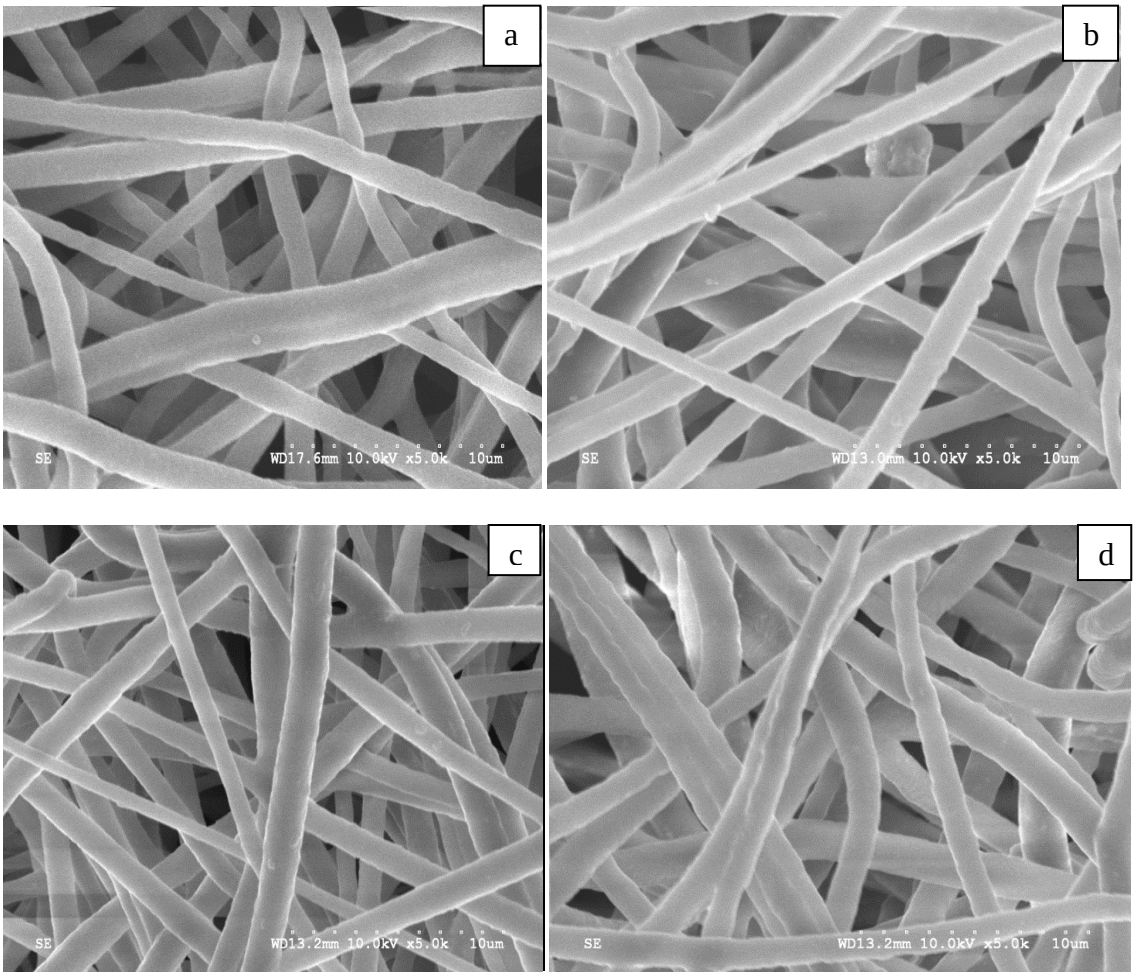

Figure 5-2: SEM images of electrospun mats with a) 2.5 wt% b) 5 wt% c) 7.5 wt% d) 10 wt% magnetite

Table 5-2: Diameters of nanofibers with magnetite of different concentrations

	Mat	Mag 2.5	Mag 5	Mag 7.5	Mag 10
Diameter (nm)	720	993	1034	1048	1138

5.2.2 Transmission Electron Microscopy (TEM)

The TEM image of the pure nanofiber are compared with one of magnetite-incorporated nanofiber as shown in Figure 5-3. It can be seen that magnetite was actually incorporated on the surface and inside the nanofibers.

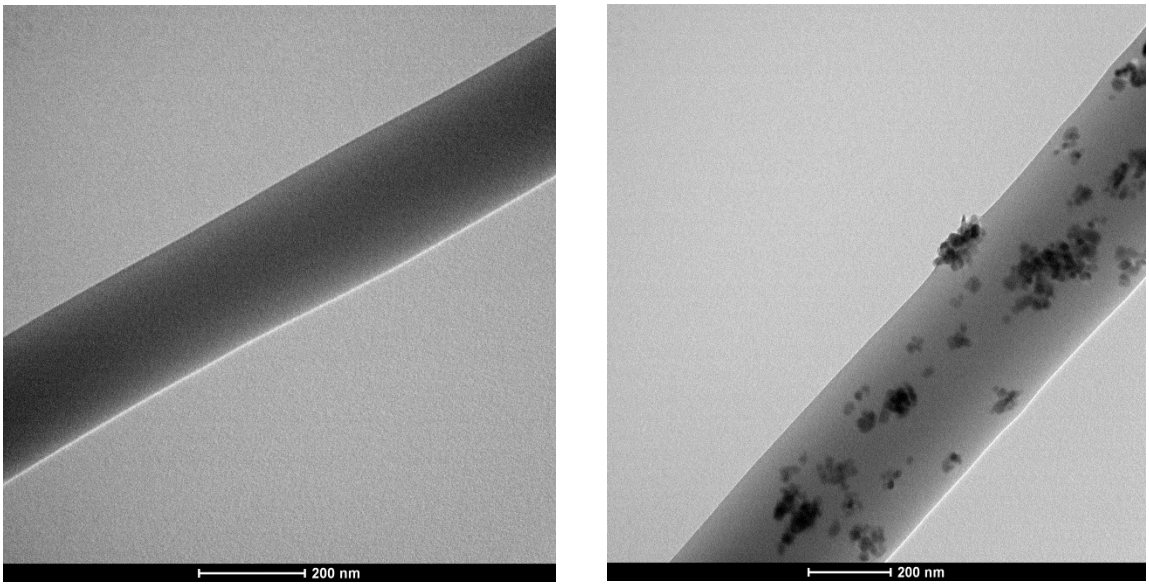

Figure 5-3: TEM images of the pure nanofiber (left) and magnetite-incorporated nanofiber (right)

5.3 Thermo-Mechanical Property

5.3.1 Differential Scanning Calorimetry (DSC)

Figure 5-4 shows the endothermic melting peaks of the soft segments in nanofiber mats with magnetite of different concentrations in the reheating (second heating) scan. Their melting point and enthalpy data are shown in table 5-3. It can be seen that the melting point and enthalpy data of magnetite-incorporated nanofiber mats were slightly lower than those of the pure nanofiber mats. This was due to the disturbance effect of the fillers

[100]. However, since the differences among them were very small, the effect of magnetite on the melting transition could be ignored.

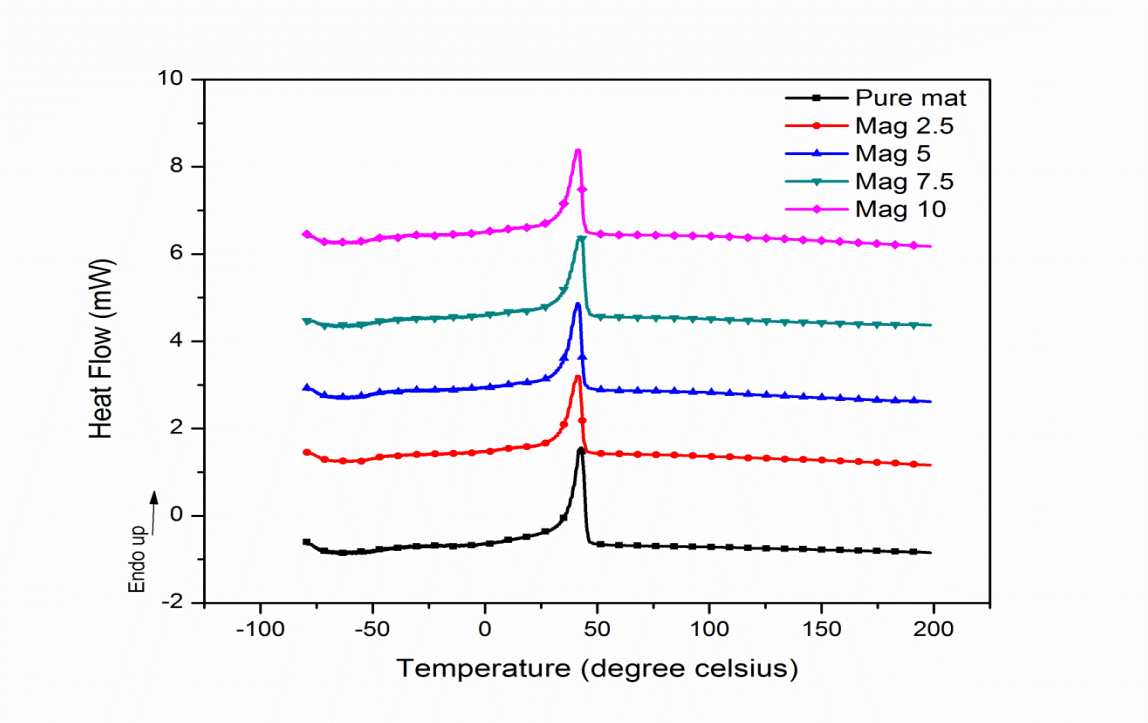

Figure 5-4: DSC curves of electrospun mats with magnetite of different concentrations

Table 5-3: DSC results of mats with magnetite of different concentrations

	T_m (℃ shown in DSC curves)	ΔH (J/g)
Nanofiber Mat	42.8	30.31
Mag 2.5	41.3	28.46
Mag 5	41.3	28.83
Mag 7.5	42.1	28.45
Mag 10	41.7	27.96

5.3.2 Dynamic Mechanical Analysis (DMA)

Figure 5-5 presents the storage modulus of nanofiber mats with different concentrations of magnetite during heating. It can be found that all of the curves were almost overlapped and the storage modulus decreased due to the melting transition of soft segments. Before transition, the modulus of all the mats was around 95 MPa. The modulus at this point was mostly attributed to physical cross-linking degrees in hard segments and the crystalline nature of soft segments [100] After transition, the storage modulus almost completely attributed to the hard segment and the amorphous phase of soft segment was very low. All of them were around 1 MPa. The melting points of different mats measured from DMA curves are shown in table 5-4, which were similar with the DSC data. Figure 5-5 and table 5-4 revealed that there was minimal change of the melting transition and themo-mechanical properties of mats after magnetite incorporation. The dramatic decreasing of storage modulus proved that there were large chances of magnetite-incorporated nonwovens to have the shape memory effect.

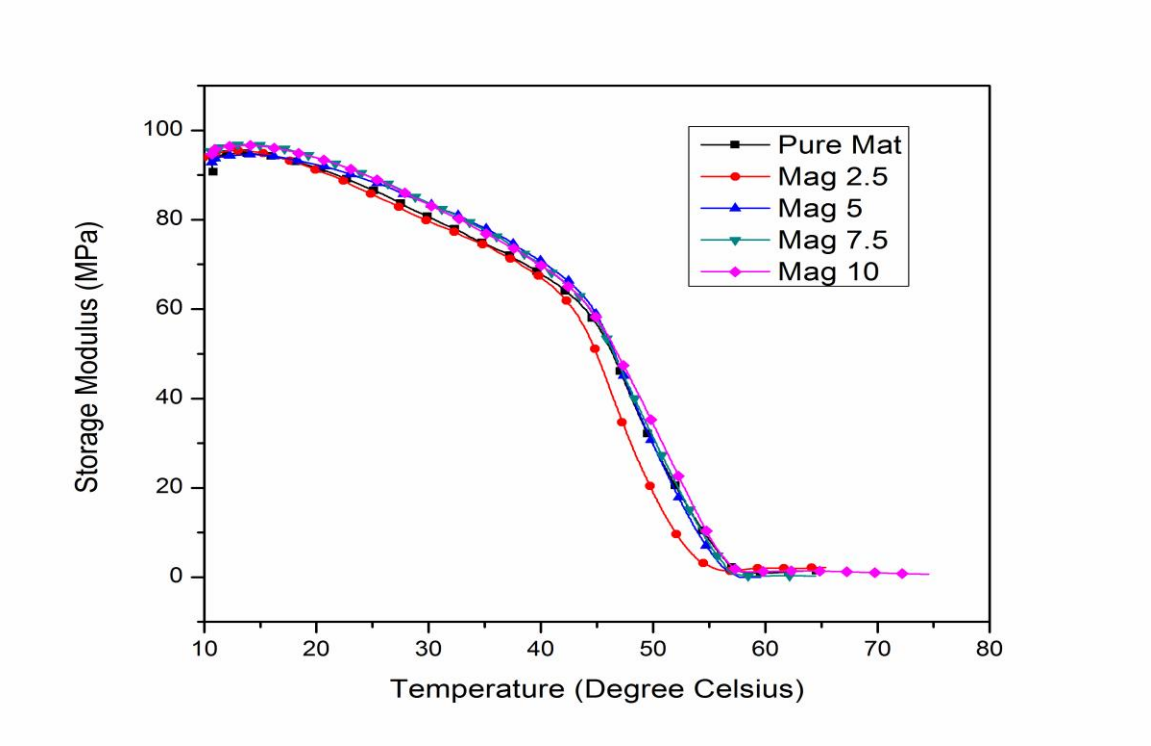

Figure 5-5: DMA curves of electrospun mats with magnetite of different concentrations

Table 5-4: DMA results of mats with magnetite of different concentrations

	Tm (℃ measured from DMA curves)	Storage Modulus at the beginning (MPa)	Storage Modulus after transition (MPa)
Nanofiber Mat	45.4	94.8	1.34
Mag 2.5	43.3	95.4	1.54
Mag 5	44.4	94.5	0.75
Mag 7.5	44.2	96.8	0.82
Mag 10	43.5	96.9	1.04

5.4 Shape Memory Property

In order to investigate the effect of magnetite on the shape memory property, cyclic tensile testing was conducted. Figure 5-6 shows the cyclic stress-strain curves for each sample. Table 5-4 shows the recovery ratio and fixity ratio calculated from the results. It can be concluded that the recovery ratio of pure mat was higher than any magnetite-incorporated mats because magnetite inside fibers without the shape memory effect would disturb the polyurethane matix continuity [81]. However, the recovery ratio was usually above 70% after three cycles. In terms of fixity ratio, they were all close and above 85%, due to similarity of crystallinity of soft segments in all the mats.

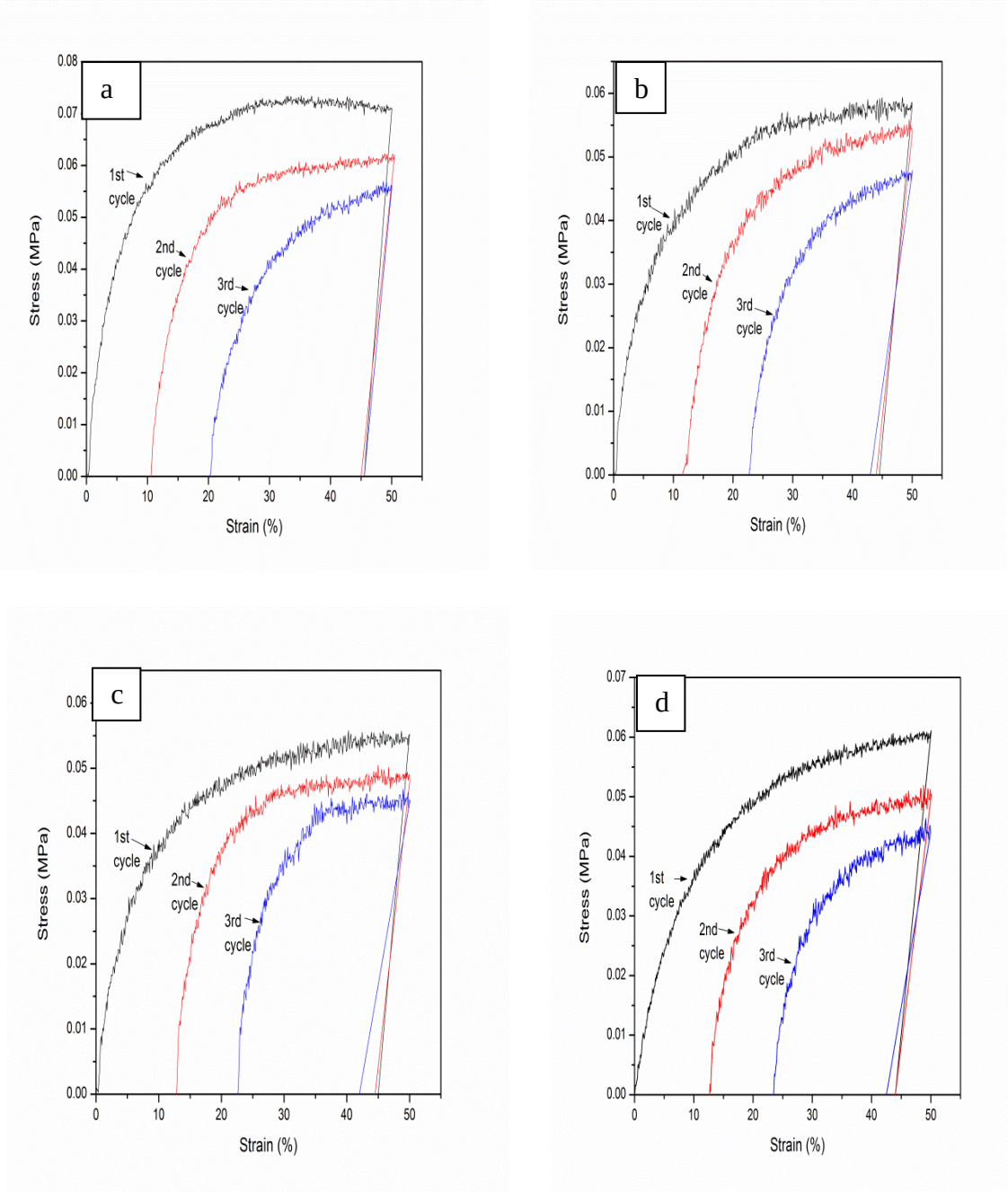

Figure 5-6: Cyclic tensile stress-strain curves of different mats with a) 2.5 wt% b) 5 wt% c) 7.5 wt% d) 10 wt% magnetite

Table 5-5: Recovery ratio and fixity ratio of mats with magnetite of different concentrations

		Mat	Mag 2.5	Mag 5	Mag 7.5	Mag 10
Recovery Ratio （%）	1st	86±2	79±1	77±5	75±1	75±3
	2nd	87±5	76±5	74±2	73±1	71±4
	3rd	91±4	73±3	74±6	72±2	69±5
Fixity Ratio (%)	1st	90±5	91±2	89±2	90±3	88±8
	2nd	93±4	90±4	88±2	89±1	88±2
	3rd	94±2	91±5	86±8	85±3	85±1

5.5 Magnetic Actuation

5.5.1 Magnetic Heating Testing

As mention in Chapter 2, the temperature of magnetite-incorporated shape memory materials can be increased due to hysteresis loss. The temperatures of different mats over time under magnetic field (strength of 0.03T and frequency of 410 kHz) within two minutes are shown in Figure 5-7. It is shown that the pure mat could not be heated up and all mats with magnetite were able to be heated in different scales. In the first section of heating, this was a linear behavior where the temperature increased quickly and later on became slow due to heat dissemination from the sample to surrounding materials.

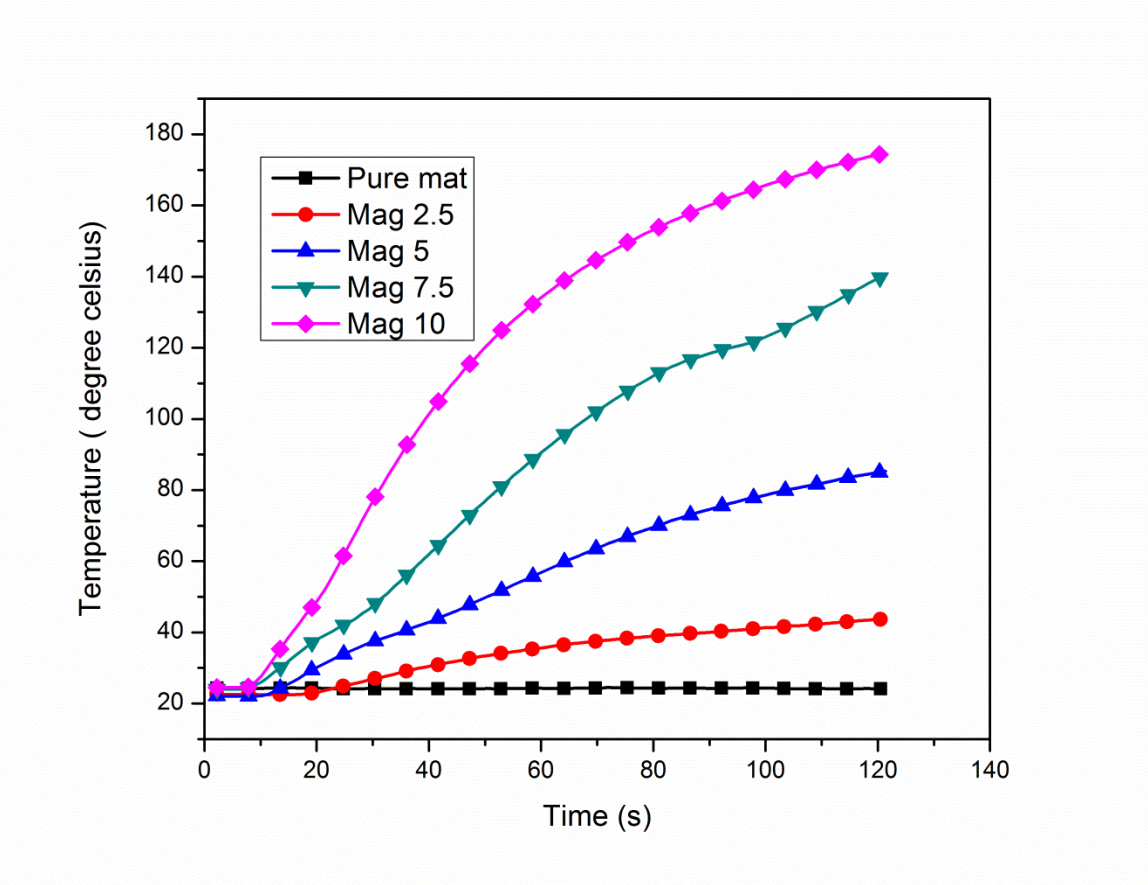

Figure 5-7: Temperature-time graphs of electrospun mats with magnetite of different concentrations

Figure 5-8 shows the relationship between increased temperatures in two minutes and magnetite concentrations, which was almost linear[102]. Here is the explanation. With higher concentration, more ferromagnetic nanoparticles took effect under magnetic field. Therefore, mats with magnetic of higher concentrations were able to absorb more hysteresis loss per a unit mass, resulting in higher heating rate [94]. As for mag 5, mag 7.5, mag 10, they were all able to reach the transition temperature, providing large possibilities for realization of the shape memory effect under a magnetic field.

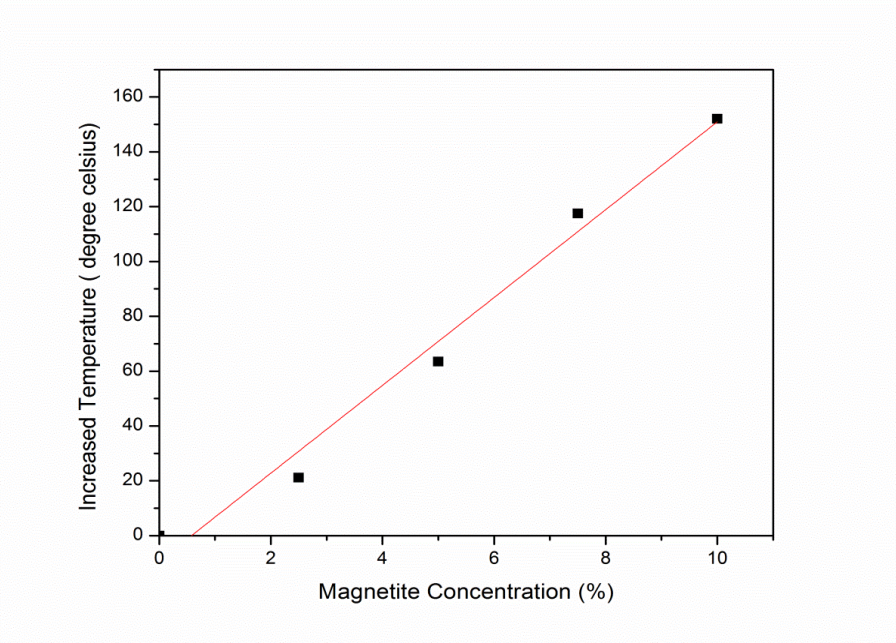

Figure 5-8: Increased temperatures of electrospun shape memory mats with magnetite of different concentrations within two minutes under a magnetic field

5.5.2 Visual Demonstration of Shape Memory Effect under Magnetic Field

In order to directly demonstration magnetic actuation of shape memory effect, the rectangular mat with 5 wt% magnetite was fixed to be helix. It was then put in the middle of a coil which generated magnetic field. Under a magnetic field with strength of 0.03T at frequency of 410 kHz, it was expected to recover to be rectangular again. Figure 5-9 shows the entire recovery process of this helix mat and Figure 5-10 shows the enlarged mats in the middle of that coil during this process. Figure 5-11 records the temperature of this mat over time. As the maximal temperature was limited to 52 ℃, the heating rate was lower than the heating curve shown in Figure 5-7. The mat initiated recovery at 70s when the temperature reached 37 ℃ and kept on changing until 120 s. The temperature

was around 45 ℃ at 120s. This process demonstrates that the shape memory effect of magnetite-incorporated nanofiber mats can be actuated under magnetic field. However, the recovery was not very complete. There are two reasons to explain this observation. First, the recovery ratio itself calculated from cyclic tensile testing was 70-80%, which was not particularly high. On the other hand, the unrecovered parts were actually the two ends of this sample which needed longest time to recover. When the temperature was above the transition temperature, after other parts had been recovered these two parts were unable to recover well before the mat became very soft and sticky.

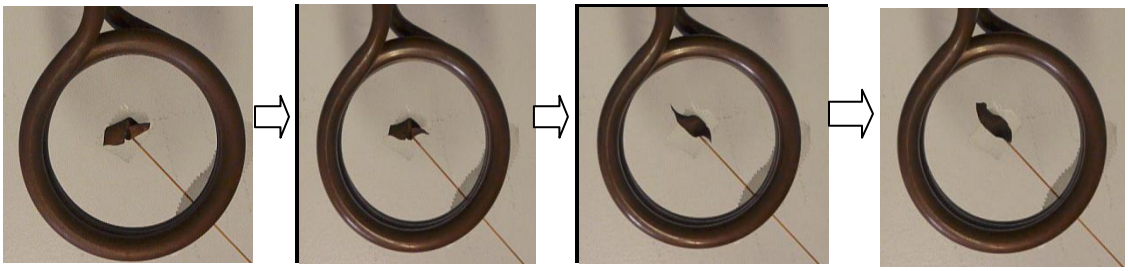

0 S 70 S 100 S 120 S

Figure 5-9: Helix recovery process of electrospun shape memory mats with 5 wt% magnetite (including coils and the mat)

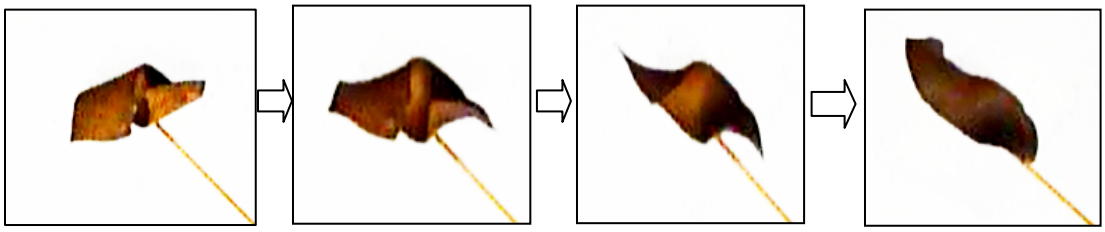

0 S 70 S 100 S 120 S

Figure 5-10: Helix recovery process of electrospun shape memory mats with 5 wt% magnetite (enlarged photos)

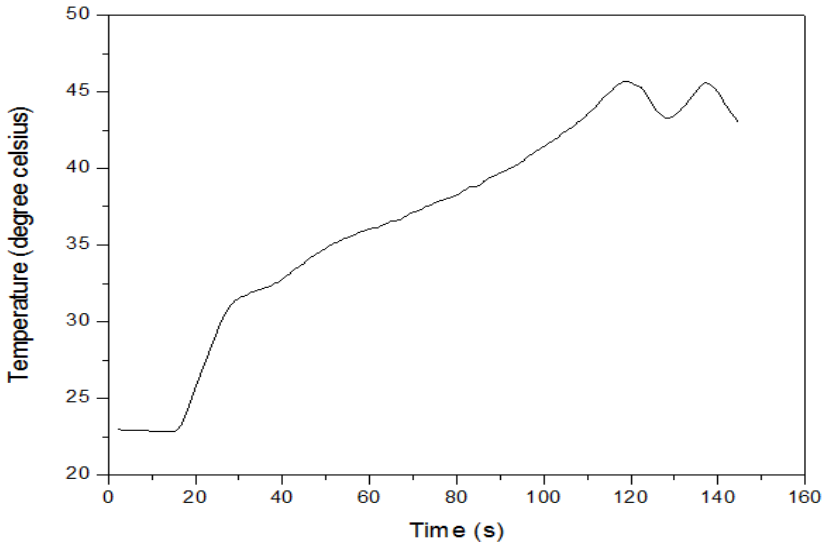

Figure 5-11: Temperature-time graph during the helix recovery process

5.6 Conclusions

In this chapter, magnetite was successfully incorporated into polyurethane shape memory nonwovens through sonic mixing and electrospinning, as verified by x-ray diffraction. The nanofibers became more uniform and the diameter increased slightly after magnetite incorporation as shown in SEM images. Furthermore, magnetite nanoparticles were observed on the surface and inside of fibers by means of transmission electron microscope. Moreover, differential scanning calorimetry and dynamic mechanical analysis revealed that there was minimal change of the melting transition of the soft phase and the thermo-mechanical properties of mats after magnetite incorporation when the concentration was below 10%. Through cyclic tensile testing, it can be concluded that recovery ratio decreased slightly due to the disturbance of magnetite on polyurethane

matrix continuity, but it was still above 70%. Magnetic heating tests proved that nanofiber mats with 5 wt%, 7.5 wt%, and 10 wt% magnetite could be heated to above the transition temperature under a magnetic field with strength of 0.03T at frequency of 410 kHz. The helix nanofiber mat with 5 wt% magnetite under the same magnetic field used in magnetic heating tests recovered to the primary rectangular shape, directly demonstrating the magnetic actuation of magnetite-incorporated electrospun shape memory mats.

Chapter 6: Conclusions and Future Work

6.1 Conclusions

The magnetic actuation of magnetite-incorporated shape memory nanofiber nonwovens was successfully achieved with minimal disturbance effect of magnetite on various properties when the concentration was below 10 wt%.

In the first stage, the polyurethane shape memory nanofiber nonwovens were fabricated and characterized. In comparison with shape memory bulk films, nanofiber mats had better recoverability attributed to molecular orientation. In the second stage, magnetite was successfully incorporated into polyurethane shape memory nonwovens through an electrospinnig process. Scanning electron microscopy showed that fibers became more uniform and the diameter increased slightly after magnetite incorporation. Differential scanning calorimetry and dynamic mechanical analysis revealed that the magnetite-incorporated mat still featured the melting transition which was similar with the pure mats, providing them the large possibilities to have shape memory effect. Through cyclic tensile testing, recovery ratio decreased slightly due to disturbance of magnetite on polyurethane matrix continuity. Furthermore, nanofiber mats with concentration of 5 wt%, 7.5 wt% and 10 wt% were able to be heated up to above transition temperature under a magnetic field with strength of 0.03T and frequency of 410 kHz. Finally, the helix nanofiber mat with 5 wt% magnetite under the same magnetic field used in

magnetic heating tests recovered to the primary rectangular shape, directly demonstrating the magnetic actuation of magnetite-incorporated electrospun shape memory mats.

Magnetic-actuated electrospun shape memory mats hold great potential for biomedical applications such as scaffolds in tissue engineering and drug delivery matrix in drug releasing system.

6.2 Challenges and Future Work

This study has set foundations for the work that can be done in the future, as suggested in the following.

1) The current work utilizes the electrospun nonwoven mats to realize shape recovery. Based on this, different fibrous structures can be fabricated such as woven fabric, knitted faric and so on. In order to apply them to specific applications, various shapes based on different fabrious structures can be designed.
2) One of the biggest problems is the difficulty in maintaining the fibrous structure in the cyclic shape memory process. As a part of this system is melting, nanofiber mats become very soft and sticky above the transition temperature. After some cycles, the fibrous structure would be destroyed. Therefore, how to avoid the fusion of fibrous structure and how to extend the shape memory cycle life needs to be addressed.
3) This study is only focused on dual-shape which contains one temporary shape. Thus, in the future, pursuing multiple shapes instead of dual shape might be a promising direction.

4) The reversible shape memory effect can be realized to take over the one-way shape memory effect in the future.
5) Different kinds of shape memory polymers can be explored to be used in shape memory nanofiber area.
6) Considering the big potential of biomedical applications, the work related to biomedical applications must be taken into account. One possibility would be adjustment of the transition temperature to be close to the body temperature. Changing the composition percentage of soft segments and hard segments might be a good option to realize the adjustment. If these devices need to be actuated by indirect heating (not just by body heat), heat transfer from the SMP to the adjacent fluid and tissue might need to be addressed.

Bibliography

[1] A. Lendlein and S. Kelch, "Shape-Memory Effect," *Angew. Chem. Int. Ed.*, vol. 41, pp. 2034–2057, 2002.

[2] C. Liu, H. Qin, and P. T. Mather, "Review of progress in shape-memory polymers," *J. Mater. Chem.*, vol. 17, p. 1543, 2007.

[3] F. El Feninat and G. Laroche, "Shape memory materials for biomedical applications," *Adv. Eng. Mater.*, vol. 4, pp. 91–104, 2002.

[4] J. Van Humbeeck, "Non-medical applications of shape memory alloys," *Mater. Sci. Eng. A*, vol. 273–275, pp. 134–148, Dec. 1999.

[5] W. Huang, "On the selection of shape memory alloys for actuators," *Mater. Des.*, vol. 23, pp. 11–19, 2002.

[6] R. Vaidyanathan, "Shape-memory alloys," *Kirk-Othermer Encycl. Chem. Technol.*, pp. 1–13, 2002.

[7] Q. Meng, "Studies of Functional Shape Memory Fibers," *PolyU Institutional Repository*, 2010.

[8] W. Huang and B. Yang, "Polyurethane Shape Memory Polymers," *CRC Press*, pp. 1–6, 2012.

[9] W. Small, P. Singhal, S. Wilson, and D. J. Maitland, "Biomedical applications of thermally activated shape memory polymers †," *J. Mater. Chem.*, vol. 20, pp. 3356–3366, 2010.

[10] I. A. Rousseau, "Challenges of Shape Memory Polymers : A Review of the Progress Toward Overcoming SMP ' s Limitations," *Polym. enginerring Sci.*, p. 2076, 2008.

[11] S. Chen, J. Hu, Y. Liu, H. Liem, Y. Zhu, and Y. Liu, "Effect of SSL and HSC on Morphology and Properties of PHA Based SMPU Synthesized by Bulk Polymerization Method," *J. Polym. Sci. Part B Polym. Phys.*, vol. 45, pp. 444–454, 2007.

[12] J. Li, T. Liu, S. Xia, Y. Pan, Z. Zheng, X. Ding, and Y. Peng, "A versatile approach to achieve quintuple-shape memory effect by semi-interpenetrating polymer networks containing broadened glass transition and crystalline segments," *J. Mater. Chem.*, vol. 21, p. 12213, 2011.

[13] T. Xie, “Tunable polymer multi-shape memory effect.,” *Nature*, vol. 464, pp. 267–70, Mar. 2010.

[14] A. Lendlein, A. M. Schmidt, and R. Langer, “AB-polymer networks based on oligo-caprolactone segments showing shape-memory properties,” *PNAS*, vol. 98, pp. 842–847, 2001.

[15] Q. Meng, J. Hu, K. Ho, F. Ji, and S. Chen, “The Shape Memory Properties of Biodegradable Chitosan/Poly(l-lactide) Composites,” *J. Polym. Environ.*, vol. 17, pp. 212–224, Oct. 2009.

[16] T. Takahashi, “Structure and Properties of Shape-Memory Polyurethane,” *J. Appl. Polym. Sci.*, vol. 60, pp. 1061–1069, 1996.

[17] J. R. Lin and L. W. Chen, “Study on shape-memory behavior of polyether-based polyurethanes. I. Influence of the hard-segment content,” *J. Appl. Polym. Sci.*, vol. 69, pp. 1563–1574, Aug. 1998.

[18] B. S. Lee, B. C. Chun, Y. C. Chung, K. Il Sul, and J. W. Cho, “Structure and Thermomechanical Properties of Polyurethane Block Copolymers with Shape Memory Effect,” *Macromolecules*, vol. 34, pp. 6431–6437, Aug. 2001.

[19] C. Zhang, J. Hu, F. Ji, Y. Fan, and Y. Liu, “A combined experimental and computational study on the material properties of shape memory polyurethane.,” *J. Mol. Model.*, vol. 18, pp. 1263–71, Apr. 2012.

[20] C. Zhang, J. Hu, S. Chen, and F. Ji, “Theoretical study of hydrogen bonding interactions on MDI-based polyurethane.,” *J. Mol. Model.*, vol. 16, pp. 1391–9, Aug. 2010.

[21] C. Liu and P. T. Mather, “Thermomechanical characterization of blends of poly (vinyl acetate) with semicrystalline polymers for shape memory applications introduction :,” in *Proceedings of the Annual Technical Conference - Society of Plastics Engineers*, pp. 1962–1966, 2003.

[22] F. L. Ji, J. L. Hu, T. C. Li, and Y. W. Wong, “Morphology and shape memory effect of segmented polyurethanes. Part I: With crystalline reversible phase,” *Polymer (Guildf).*, vol. 48, pp. 5133–5145, Aug. 2007.

[23] S. Chen, Q. Cao, B. Jing, Y. Cai, P. Liu, and J. Hu, “Effect of microphase-separation promoters on the shape-memory behavior of polyurethane,” *J. Appl. Polym. Sci.*, vol. 102, pp. 5224–5231, Dec. 2006.

[24] Y. Zhu, J. L. Hu, K. W. Yeung, Y. Q. Liu, and H. M. Liem, "Influence of ionic groups on the crystallization and melting behavior of segmented polyurethane ionomers," *J. Appl. Polym. Sci.*, vol. 100, pp. 4603–4613, Jun. 2006.

[25] Y. Zhu, J. Hu, K. Yeung, K. Choi, Y. Liu, and H. Liem, "Effect of Cationic Group Content on Shape Memory Effect in Segmented Polyurethane Cationomer," *J. Appl. Polym. Sci.*, vol. 103, pp. 545–556, 2007.

[26] L. Zhang, Y. Jiang, Z. Xiong, X. Liu, H. Na, R. Zhang, and J. Zhu, "Highly recoverable rosin-based shape memory polyurethanes," *J. Mater. Chem. A*, vol. 1, p. 3263, 2013.

[27] M. Wang, "Dynamic Mechanical Behavior In the Ethylene Terephthalate-Ethylene Oxide Copolymer With Long Soft Segment as A Shape Memory Material," *Eur.Polym.*, vol. 34, pp. 1–5, 1998.

[28] T. Tong, "shape memory styrene copolymer," US 6759481, 2002.

[29] V. Beloshenko, Y. Beygelzimer, A . Borzenko, and V.Varyukhin, "Shape memory effect in the epoxy polymer–thermoexpanded graphite system," *Compos. Part A Appl. Sci. Manuf.*, vol. 33, pp. 1001–1006, Jul. 2002.

[30] C. Liu, S. B. Chun, P. T. Mather, L. Zheng, E. H. Haley, and E. B. Coughlin, "Chemically Cross-Linked Polycyclooctene: Synthesis, Characterization, and Shape Memory Behavior," *Macromolecules*, vol. 35, pp. 9868–9874, Dec. 2002.

[31] J. Hu, Z. Yang, L. Yeung, F. Ji, and Y. Liu, "Crosslinked polyurethanes with shape memory properties," *Polym. Int.*, vol. 54, pp. 854–859, May 2005.

[32] M. Anthamatten, S. Roddecha, and J. Li, "Energy Storage Capacity of Shape-Memory Polymers," *Macromolecules*, vol. 46, pp. 4230–4234, May 2013.

[33] A. Disassembly, U. Shape, F. O. R. The, and M. Phone, "Active disassembly using shape memory polymers for the mobile phone industry," *IEEE*, pp. 151–156, 1999.

[34] X. Lan, Y. Liu, H. Lv, X. Wang, J. Leng, and S. Du, "Fiber reinforced shape-memory polymer composite and its application in a deployable hinge," *Smart Mater. Struct.*, vol. 18, p. 1-6, Feb. 2009.

[35] H. M. Wache, D. J. Tartakowska, a Hentrich, and M. H. Wagner, "Development of a polymer stent with shape memory effect as a drug delivery system.," *J. Mater. Sci. Mater. Med.*, vol. 14, pp. 109–12, Feb. 2003.

[36] A. Lendlein and R. Langer, "Biodegradable, elastic shape-memory polymers for potential biomedical applications.," *Science*, vol. 296, pp. 1673–6, May 2002.

[37] C. Wischke, A. T. Neffe, S. Steuer, and A. Lendlein, "Evaluation of a degradable shape-memory polymer network as matrix for controlled drug release.," *J. Control. Release*, vol. 138, pp. 243–50, Sep. 2009.

[38] W. M. Sokolowski, "Self-Deployable Membrane Structures," *NASA Tech Briefs*, p. 14, 2010.

[39] J. Hu, H. Meng, G. Li, and S. I. Ibekwe, "A review of stimuli-responsive polymers for smart textile applications," *Smart Mater. Struct.*, vol. 21, p. 1-23, May 2012.

[40] D. J. Maitland, W. Small, J. M. Ortega, P. R. Buckley, J. Rodriguez, J. Hartman, and T. S. Wilson, "Prototype laser-activated shape memory polymer foam device for embolic treatment of aneurysms.," *J. Biomed. Opt.*, vol. 12, no. 3, p. 030504, 2014.

[41] Z. Hu, Y. Chen, C. Wang, and Y. Zheng, "Polymer gels with engineered environmentally responsive surface patterns," *Nature*, vol. 393, pp. 149–152, 1998.

[42] F. Ji, Y. Zhu, J. Hu, Y. Liu, L. Y. Yeung, and G. Ye, "Smart polymer fibers with shape memory effect," *Smart Mater. Struct.*, vol. 15, pp. 1547–1554, Dec. 2006.

[43] Q. Meng, J. Hu, Y. Zhu, J. Lu, and B. Liu, "Biological Evaluations of a Smart Shape Memory Fabric," *Text. Res. J.*, vol. 79, pp. 1522–1533, Sep. 2009.

[44] Q. Meng, J. Hu, Y. Zhu, J. Lu, and Y. Liu, "Polycaprolactone-Based Shape Memory Segmented Polyurethane Fiber," *J. Appl. Polym. Sci.*, vol. 106, pp. 2515–2523, 2007.

[45] Q. Meng and J. Hu, "A temperature-regulating fiber made of PEG-based smart copolymer," *Sol. Energy Mater. Sol. Cells*, vol. 92, pp. 1245–1252, Oct. 2008.

[46] Y. Liu, J. Lu, J. Hu, and A. Chung, "Study on the bagging behavior of knitted fabrics by shape memory polyurethane fiber," *J. Text. Inst.*, pp. 1–7, Apr. 2013.

[47] Y. Liu, A. Chung, J. Hu, and J. Lv, "Shape memory behavior of SMPU knitted fabric," *J. Zhejiang Univ. Sci. A*, vol. 8, pp. 830–834, Apr. 2007.

[48] H. Chen, X. Cao, J. Zhang, J. Zhang, Y. Ma, G. Shi, Y. Ke, D. Tong, and L. Jiang, "Electrospun shape memory film with reversible fibrous structure," *J. Mater. Chem.*, vol. 22, p. 22387, 2012.

[49] J. T. Seil and T. J. Webster, "Electrically active nanomaterials as improved neural tissue regeneration scaffolds.," *Wiley interdisciplinary reviews. Nanomedicine and nanobiotechnology*, vol. 2, pp. 635–47, 2010.

[50] V. Leung and F. Ko, “Biomedical applications of nanofibers,” *Polym. Adv. Technol.*, vol. 22, pp. 350–365, Mar. 2011.

[51] M. Ignatova, K. Starbova, N. Markova, N. Manolova, and I. Rashkov, “Electrospun nano-fibre mats with antibacterial properties from quaternised chitosan and poly(vinyl alcohol).,” *Carbohydr. Res.*, vol. 341, pp. 2098–107, Sep. 2006.

[52] H. T. Zhuo, “Coaxial electrospun polyurethane core-shell nanofibers for shape memory and antibacterial nanomaterials,” *eXPRESS Polym. Lett.*, vol. 5, pp. 182–187, Jan. 2011.

[53] W. J. Li, C. T. Laurencin, E. J. Caterson, R. S. Tuan, and F. K. Ko, “Electrospun nanofibrous structure: a novel scaffold for tissue engineering.,” *J. Biomed. Mater. Res.*, vol. 60, pp. 613–21, Jun. 2002.

[54] A. Frenot and I. S. Chronakis, “Polymer nanofibers assembled by electrospinning,” *Curr. Opin. Colloid Interface Sci.*, vol. 8, pp. 64–75, 2003.

[55] L.F. Tseng, P. T. Mather, and J. H. Henderson, “Shape-memory-actuated change in scaffold fiber alignment directs stem cell morphology.,” *Acta Biomater.*, vol. 9, pp. 8790-8801, Jul. 2013.

[56] H. Zhuo, J. Hu, and S. Chen, “Study of water vapor permeability of shape memory polyurethane nanofibrous nonwovens,” *Text. Res. J.*, vol. 81, pp. 883–891, Jan. 2011.

[57] J. S. Ahn, W. R. Yu, J. H. Youk, and H. Y. Ryu, “In situ temperature tunable pores of shape memory polyurethane membranes,” *Smart Mater. Struct.*, vol. 20, p. 105024, Oct. 2011.

[58] H. Zhuo, J. Hu, and S. Chen, “Study of water vapor permeability of shape memory polyurethane nanofibrous nonwovens,” *Text. Res. J.*, vol. 81, pp. 883–891, Jan. 2011.

[59] F. Ko and Y. Wan, "Introduction to Nanofiber Materials," *Cambridge University Press*, p. 39, 2014.

[60] S. E. Chung, C. H. Park, W. Yu, and T. J. Kang, “Thermoresponsive Shape Memory Characteristics of Polyurethane Electrospun Web,” *J. Appl. Polym. Sci.*, vol. 120, pp. 492–500, 2011.

[61] J. N. Zhang, Y. M. Ma, J. J. Zhang, D. Xu, Q. L.Yang, J. G. Guan, X.Y. Cao, and L. Jiang, “Microfiber SMPU film affords quicker shape recovery than the bulk one,” *Mater. Lett.*, vol. 65, pp. 3639–3642, Dec. 2011.

[62] Q. Meng, J. Hu, Y. Zhu, J. Lu, and Y. Liu, “Morphology, phase separation, thermal and mechanical property differences of shape memory fibres prepared by different spinning methods,” *Smart Mater. Struct.*, vol. 16, pp. 1192–1197, Aug. 2007.

[63] H. Zhuo, J. Hu, and S. Chen, “Electrospun polyurethane nanofibres having shape memory effect,” *Mater. Lett.*, vol. 62, pp. 2074–2076, May 2008.

[64] D. Ratna and J. Karger-Kocsis, “Recent advances in shape memory polymers and composites: a review,” *J. Mater. Sci.*, vol. 43, pp. 254–269, Oct. 2007.

[65] K. Nagahama, Y. Ueda, T. Ouchi, and Y. Ohya, “Biodegradable shape-memory polymers exhibiting sharp thermal transitions and controlled drug release.,” *Biomacromolecules*, vol. 10, pp. 1789–94, Jul. 2009.

[66] Q. Meng and J. Hu, “Self-organizing alignment of carbon nanotube in shape memory segmented fiber prepared by in situ polymerization and melt spinning,” *Compos. Part A Appl. Sci. Manuf.*, vol. 39, pp. 314–321, Feb. 2008.

[67] S. Rana and J. W. Cho, “Core-sheath polyurethane-carbon nanotube nanofibers prepared by electrospinning,” *Fibers Polym.*, vol. 12, pp. 721–726, Sep. 2011.

[68] Y. Zhu, J. Hu, L. Y. Yeung, Y. Liu, F. Ji, and K. Yeung, “Development of shape memory polyurethane fiber with complete shape recoverability,” *Smart Mater. Struct.*, vol. 15, pp. 1385–1394, Oct. 2006.

[69] Y. Zhu, J. Hu, J. Lu, L. Y. Yeung, and K. Yeung, “Shape memory fiber spun with segmented polyurethane ionomer,” *Polym. Adv. Technol.*, vol. 19, pp. 1745–1753, 2008.

[70] H. R. Han, S. E. Chung, and C. H. Park, “Shape memory and breathable waterproof properties of polyurethane nanowebs,” *Text. Res. J.*, vol. 83, no. 1, pp. 76–82, Sep. 2012.

[71] F. Zhang, Z. Zhang, Y. Liu, and J. Leng, “Fabrication of shape memory nanofibers by electrospinning method,” *Electroact. Polym. Actuators Devices*, vol. 8687, Apr. 2013.

[72] H. Matsumoto, T. Ishiguro, Y. Konosu, M. Minagawa, A. Tanioka, K. Richau, K. Kratz, and A. Lendlein, “Shape-memory properties of electrospun non-woven fabrics prepared from degradable polyesterurethanes containing poly(ω-pentadecalactone) hard segments,” *Eur. Polym. J.*, vol. 48, pp. 1866–1874, Nov. 2012.

[73] P. K. Baumgarten, “Electrostatic spinning of acrylic microfibers,” *J. Colloid Interface Sci.*, vol. 36, pp. 71–79, May 1971.

[74] S. J. Pomfret, P. N. Adams, N. P. Comfort, and A. P. Monkman, “Electrical and mechanical properties of polyaniline fibres produced by a one-step wet spinning process ☪,” *Polymer (Guildf).*, vol. 41, pp. 2265–2269, 2000.

[75] Q. Meng, J. Liu, L. Shen, Y. Hu, and J. Han, “A Smart Hollow Filament with Thermal Sensitive Internal Diameter,” *J. Appl. Polym. Sci.*, vol. 113, pp. 2440–2449, 2009.

[76] Q. Meng and J. Hu, “Study on poly (e -caprolactone) -based shape memory copolymer fiber prepared by bulk polymerization and melt spinning,” *Polym. Adv. Technol*, vol. 19, pp. 131–136, 2008.

[77] A. Sharp, H. V Panchawagh, A. Ortega, R. Artale, S. Richardson-Burns, D. S. Finch, K. Gall, R. L. Mahajan, and D. Restrepo, “Toward a self-deploying shape memory polymer neuronal electrode.,” *J. Neural Eng.*, vol. 3, pp. L23–30, Dec. 2006.

[78] Q. Meng and J. Hu, “A review of shape memory polymer composites and blends,” *Compos. Part A Appl. Sci. Manuf.*, vol. 40, pp. 1661–1672, Nov. 2009.

[79] C. Ayranci, H. Yang, and F. Ko, “Self-activated Carbon Fiber Reinforced Shape Memory Polymer Composites,” in *26th Annual Technical Conference of the American Society for Composites 2011 and the 2nd Joint US-Canada Conference on Composites*, pp. 442–450, 2011.

[80] C. Ayranci, F. Ko, and T. Howie, “Shape memory effect of a thermoset polymer and its,” in *18th International Conference on Composite Materials*, pp. 1–5, 2011.

[81] Q. Meng, J. Hu, and L. Yeung, “An electro-active shape memory fibre by incorporating multi-walled carbon nanotubes,” *Smart Mater. Struct.*, vol. 16, pp. 830–836, Jun. 2007.

[82] S. Rana, S. D. Kim, and J. W. Cho, “Conducting core-sheath nanofibers for electroactive shape-memory applications,” *Polym. Adv. Technol.*, vol. 24, pp. 609–614, Jul. 2013.

[83] A. M. Schmidt, “Electromagnetic Activation of Shape Memory Polymer Networks Containing Magnetic Nanoparticles,” *Macromol. Rapid Commun.*, vol. 27, pp. 1168–1172, Jul. 2006.

[84] W. Small, M. F. Metzger, T. S. Wilson, and D. J. Maitland, “Laser-activated shape memory polymer microactuator for thrombus removal following ischemic stroke:

preliminary in vitro analysis," *IEEE J. Sel. Top. Quantum Electron.*, vol. 11, pp. 892–901, Jul. 2005.

[85] D. J. Maitland, M. F. Metzger, D. Schumann, A. Lee, and T. S. Wilson, "Photothermal Properties of Shape Memory Polymer Micro-Actuators for Treating Stroke," *Lasers Surg. Med.*, vol. 30, pp. 1–11, 2002.

[86] H. Koerner, G. Price, N. a Pearce, M. Alexander, and R. a Vaia, "Remotely actuated polymer nanocomposites--stress-recovery of carbon-nanotube-filled thermoplastic elastomers.," *Nat. Mater.*, vol. 3, pp. 115–20, Feb. 2004.

[87] S. Dutz and R. Hergt, "Magnetic particle hyperthermia: nanoparticle magnetism and materials development for cancer therapy" *J. Phas.: Condens. Matter*, vol. 18, no. 38, pp. 2919-2934, 2006.

[88] S. Dutz and R. Hergt, "Magnetic nanoparticle heating and heat transfer on a microscale: Basic principles, realities and physical limitations of hyperthermia for tumour therapy.," *Int. J. Hyperthermia*, vol. 29, pp. 790–800, Dec. 2013.

[89] R. Hergt and S. Dutz, "Magnetic particle hyperthermia—biophysical limitations of a visionary tumour therapy," *J. Magn. Magn. Mater.*, vol. 311, pp. 187–192, Apr. 2007.

[90] C. M. Yakacki, N. S. Satarkar, K. Gall, R. Likos, and J. Z. Hilt, "Shape-Memory Polymer Networks with Fe 3 O 4 Nanoparticles for Remote Activation," *J. Appl. Polym. Sci.*, vol. 112, pp. 3166–3176, 2009.

[91] R. Mohr, K. Kratz, T. Weigel, M. Moneke, and A. Lendlein, "Initiation of shape-memory effect by inductive heating of magnetic nanoparticles," *PANS*, vol. 103, pp. 3540–3545, 2006.

[92] T. Weigel, R. Mohr, and a Lendlein, "Investigation of parameters to achieve temperatures required to initiate the shape-memory effect of magnetic nanocomposites by inductive heating," *Smart Mater. Struct.*, vol. 18, Feb. 2009.

[93] X. Yu, S. Zhou, X. Zheng, T. Guo, Y. Xiao, and B. Song, "A biodegradable shape-memory nanocomposite with excellent magnetism sensitivity.," *Nanotechnology*, vol. 20, no. 235702, Jun. 2009.

[94] T. Gong, W. Li, H. Chen, L. Wang, S. Shao, and S. Zhou, "Remotely actuated shape memory effect of electrospun composite nanofibers.," *Acta Biomater.*, vol. 8, pp. 1248–59, Mar. 2012.

[95] Y. Cai, J. S. Jiang, Z. W. Liu, Y. Zeng, and W. G. Zhang, "Magnetically-sensitive shape memory polyurethane composites crosslinked with multi-walled carbon nanotubes," *Compos. Part A Appl. Sci. Manuf.*, vol. 53, pp. 16–23, Oct. 2013.

[96] U. N. Kumar, K. Kratz, W. Wagermaier, M. Behl, and a. Lendlein, "Non-contact actuation of triple-shape effect in multiphase polymer network nanocomposites in alternating magnetic field," *J. Mater. Chem.*, vol. 20, p. 3404, 2010.

[97] P. R. Buckley, G. H. McKinley, T. S. Wilson, W. Small, W. J. Benett, J. P. Bearinger, M. W. McElfresh, and D. J. Maitland, "Inductively heated shape memory polymer for the magnetic actuation of medical devices.," *IEEE Trans. Biomed. Eng.*, vol. 53, pp. 2075–83, Oct. 2006.

[98] Y. Zhu, J. Hu, K. Choi, K. Yeung, Q. Meng, and S. Chen, "Crystallization and Melting Behavior of the Crystalline Soft Segment in a Shape-Memory Polyurethane Ionomer," *Journal of Applied Polymer Science*, vol. 107, pp. 599-609, 2007.

[99] L. Averous, L. Moro, P. Dole, and C. Fringant, "Properties of thermoplastic blends : starch – polycaprolactone," *Polymer (Guildf).*, vol. 41, pp. 4157–4167, 2000.

[100] X. Wang, J. Zhao, M. Chen, L. Ma, X. Zhao, Z. M. Dang, and Z. Wang, "Improved self-healing of polyethylene/carbon black nanocomposites by their shape memory effect.," *J. Phys. Chem. B*, vol. 117, pp. 1467–74, Feb. 2013.

[101] H. Zhuo, J. Hu, and S. Chen, "Study of the thermal properties of shape memory polyurethane nanofibrous nonwoven," *J. Mater. Sci.*, vol. 46, pp. 3464–3469, Jan. 2011.

[102] B. Kozissnik, A. C. Bohorquez, J. Dobson, and C. Rinaldi, "Magnetic fluid hyperthermia: advances, challenges, and opportunity.," *Int. J. Hyperth.*, vol. 29, pp. 706–14, Dec. 2013.